Sun-induced Chlorophyll fluorescence and PRI improve remote sensing GPP estimates under varying nutrient availability in a typical Mediterranean savanna ecosystem

Oscar Perez-Priego[1]*, Jinhong Guan[1,2], Micol Rossini[3], Francesco Fava[3], Thomas Wutzler[1], Gerardo Moreno[4], Nuno Carvalhais[1,5], Arnaud Carrara[6], Olaf Kolle[1], Tommaso Julitta[3], Marion Schrumpf[1], Markus Reichstein[1] and Mirco Migliavacca[1]*

[1] Max Planck Institute for Biogeochemistry, Jena, Germany
[2] Chinese Academy of Sciences and Ministry of Water Resources, State Key Laboratory of Soil Erosion and Dryland Farming on Loess Plateau, Institute of Soil and Water Conservation, Yangling, Shaanxi, China
[3] Università degli Studi Milano-Bicocca, Remote Sensing of Environmental Dynamics Laboratory, DISAT, Milan, Italy
[4] Universidad de Extremadura, Forest Research Group, Plasencia, 10600, Spain
[5]Departamento de Ciencias e Engenharia do Ambiente, DCEA, Faculdade de Ciencias e Tecnologia, FCT, Universidade Nova de Lisboa, 2829-516 Caparica, Portugal
[6] Fundación Centro de Estudios Ambientales del Mediterráneo (CEAM), Valencia, Spain

Oscar Perez-Priego[1]**, email: opriego@bgc-jena.mpg.de

Jinhong Guan[1,2], email: *jguan@bgc-jena.mpg.de*

Francesco Fava[3], email: *francesco.fava@unimib.it*

Micol Rossini[3], email: micol.rossini@unimib.it

Thomas Wutzler[1], email: thomas.wutzler@bgc-jena.mpg.de

Gerardo Moreno[4], email: gmoreno@unex.es

Tommaso Julitta[3], email: tommaso.julitta@gmail.com

Nuno Carvalhais[1,5], email: ncarval@bgc-jena.mpg.de

Arnaud Carrara[6], email: arnaud@ceam.es

Olaf Kolle[1], email: olaf.kolle@bgc-jena.mpg.de

Marion Schrumpf[1], email: mschrumpf@bgc-jena.mpg.de

Markus Reichstein[1], *email: mreichstein@bgc-jena.mpg.de*

Mirco Migliavacca[1], *email: mmiglia@bgc-jena.mpg.de*

Running title: Remote sensing-based model of photosynthesis

Received: May 2015

Keywords: Photochemical reflectance index, sun-induced fluorescence, nutrient availability, photosynthesis, LUE model, dehesa.

*Corresponding Author
Biosphere-Atmosphere Interactions and Experimentation group
Biogeochemical Integration Department
Max Planck Institute for Biogeochemistry,
Jena
Germany
e-mail: opriego@bgc-jena.mpg.de

Abstract

This study investigates the performances of different optical indices to estimate gross primary production (GPP) of herbaceous stratum in a Mediterranean savanna with different Nitrogen (N) and Phosphorous (P) availability. Sun-induced chlorophyll Fluorescence yield computed at 760 nm (Fy760), scaled-photochemical reflectance index (sPRI), MERIS terrestrial-chlorophyll index (MTCI) and Normalized difference vegetation index (NDVI) were computed from near-surface field spectroscopy measurements collected using high spectral resolution spectrometers covering the visible near-infrared regions. GPP was measured using canopy-chambers on the same locations sampled by the spectrometers. We tested whether light-use efficiency (LUE) models driven by remote sensing quantities (RSM) can better track changes in GPP caused by nutrient supplies compared to those driven exclusively by meteorological data (MM). Particularly, we compared the performances of different RSM formulations -relying on the use of Fy760 or sPRI as proxy for LUE and NDVI or MTCI as fraction of absorbed photosynthetically active radiation (*f*APAR) - with those of classical MM.

Results showed higher GPP in the N fertilized experimental plots during the growing period. These differences in GPP disappeared in the drying period when senescence effects masked out potential differences due to plant N content. Consequently, although MTCI was tightly related to the mean of plant N content across treatment (r^2=0.86, *p<0.01*), it was poorly related to GPP (r^2=0.45, *p*<0.05). On the contrary sPRI and Fy760 correlated well with GPP during the whole measurement period. Results revealed that the relationship between GPP and Fy760 is not unique across treatments but it is affected by N availability. Results from a cross-validation analysis showed that MM (AIC_{cv}=127, ME_{cv}= 0.879) outperformed RSM (AIC_{cv}=140, ME_{cv}= 0.8737) when soil moisture was used to constrain the seasonal dynamic of LUE. However, residual analyses demonstrated that GPP predictions with MM are

71 inaccurate whenever no climatic variable explicitly reveals nutrient-related changes in the
72 LUE parameter. These results put forward that RSM is a valuable means to diagnose nutrient-
73 induced effects on the photosynthetic activity.

74

1. Introduction

Human-induced nutrient imbalances are affecting essential processes that lead to important changes in ecosystem structure and functioning (Peñuelas et al., 2013). In spite of the crucial role of nutrients in regulating plant processes, efforts to describe and predict the response of photosynthesis to such changes with remote sensing information have been limited. In the framework of the classical Monteith Light Use Efficiency (LUE) model (Monteith, 1972), estimates of photosynthesis (hereafter gross primary productivity, GPP) are based on three key quantities: i) the fraction of photosynthetically active radiation (*f*APAR) absorbed by the vegetation, ii) potential LUE (or maximum, LUE_m), normally taken from look-up tables and associated with plant functional types (Heinsch et al., 2006) and iii) correction factors related to meteorological conditions that limit LUE_m. Although Nitrogen (N) deficiencies have been recognized one of the main correction factors of LUE_m (Madani et al., 2014), the predictive capability of LUE models is usually circumspect as they operate based on the general assumption that plants are under non-limiting nutrient conditions.

Very little attention has been given to nutrient-induced effects on *f*APAR and LUE in common formulations of LUE models. Light absorption by plant is given by chlorophyll pigments that enable photosynthetic processes. Assuming a correlation between leaf chlorophyll pigments and leaf N content, note that N atoms are basic components of the chlorophylls molecular structure, several studies have demonstrated that leaf N content can be estimated through chlorophyll-related hyperspectral vegetation indices (Baret et al., 2007; Schlemmer et al., 2013). Among these indices, the MERIS Terrestrial Chlorophyll Index (MTCI, Dash and Curran, 2004) has been used as a proxy for *f*APAR (Rossini et al., 2010; Wang et al., 2012). However, leaf N content is functional trait that controls GPP not only because it scales with chlorophylls but also regulates enzyme kinetic processes driving photosynthesis and hence the physiological status of the plant (Huang et al., 2004; Walker et

al., 2014). Then, prescribing biome-specific LUE parameters and correcting LUE_m only for climatic and environmental conditions may hamper the accurate prediction of GPP (Yuan et al., 2014). For these reasons, recent literature has called for better physiological descriptors of the dynamic behavior of LUE (Guanter et al., 2014).

The sun-induced chlorophyll fluorescence (SIF) or physiological-related reflectance indices such as the photochemical reflectance index (PRI) provide a new optical means to spatially infer LUE (Damm et al., 2010; Guanter et al., 2014; Rossini et al., 2015) and can provide diagnostic information regarding plant nutrient and water status (Lee et al., 2013; Pérez-Priego et al., 2005; Suárez et al., 2008; Tremblay et al., 2012). From a physiological perspective, the efficiency of green plants to transform absorbed light into chemical energy during photosynthesis can be characterized by two main photo-protective mechanisms: i) non-photochemical quenching that can be detected using the Photochemical Reflectance Index (PRI), originally proposed by (Gamon et al., 1992) to track changes in the de-epoxidation state of the xanthophyll cycle pigments, and ii) Chlorophyll fluorescence, the dissipation of energy that exceeds photosynthetic demand (Krause and Weis, 1984). The PRI has been directly correlated with LUE (Drolet et al., 2008; Gamon et al., 1997; Nichol et al., 2000; Peñuelas et al., 2011; Rahman et al., 2004). However, such relation may vary because of the sensitivity of the PRI to confounding factors like those associated with temporal changes in the relative fraction of chlorophyll:carotenoids pigment composition (Filella et al., 2009; Porcar-Castell et al., 2012), viewing angles and vegetation structure (Garbulsky et al., 2011; Grace et al., 2007; Hall et al., 2008; Hilker et al., 2008).

Alternatively, the estimation of SIF by passive remote sensing systems has been proven feasible in recent years from satellite (Frankenberg et al., 2014; Lee et al., 2013; Parazoo et al., 2014) to the field (Damm et al., 2010; Guanter et al., 2013; Meroni et al., 2011), and opens further possibilities to directly track the dynamics of LUE (Damm et al.,

2010; Guanter et al., 2014). Although SIF correlates with LUE, such relations might not be conservative since chlorophyll fluorescence emission varies among species types (Campbell et al., 2008) or with stress conditions such as nutrient deficiencies (Huang et al., 2004; McMurtrey et al., 2003) or drought (Flexas et al., 2002; Pérez-Priego et al., 2005). Likewise with the PRI, the retrieval of SIF from the apparent reflectance signal is not trivial as long as it is affected by the vegetation structure or canopy background components (Zarco-Tejada et al., 2013).

Comparable spatial and temporal resolutions of radiometric and ground-based GPP measurements are essential to accurately optimize LUE model parameters, particularly in heterogeneous ecosystems. Previous studies have related ecosystem-scale eddy covariance fluxes to radiometric measurements taken in single points to constraint LUE models. However, the explanatory power of LUE models might be greatly reduced by the spatial mismatch between radiometric and eddy covariance flux footprints (Gelybó et al., 2013; Porcar-Castell et al., 2015). Similar issues occur in small-scale factorial experiments where comparable measurements on an intermediate scale between leaf-scale cuvette measurements and ecosystem-scale eddy covariance measurements are required. Here, we tried to overcome such limitations by combining ground-based radiometric and CO_2 fluxes measurements with similar extension of the measurement footprint using portable spectrometers and canopy chambers in a nutrient-manipulation experiment.

The main objective of this study was to evaluate whether traditional LUE models driven by meteorological and phenological data (MM) entail a limited assessment of the environmental controls on GPP. More particularly, we evaluated if the effects of varying nutrient availability on GPP estimates as tracked by chlorophyll fluorescence and PRI can be equally explained by meteorology-driven models. To address the main objective we:

a) assess the effect of different nutrient supplies on grassland photosynthesis and optical properties and their relationships during a phenological cycle, including both growing and drying periods,

b) evaluate the performance of different LUE modeling approaches with varying nutrient availability and environmental conditions.

2. Material and Methods

2.1. Site description and experimental design

A Small scale nutrient Manipulation Experiment (SMANIE) was set up in a Mediterranean savannah in Spain (39°56'24.68"N, 5°45'50.27"W; Majadas de Tietar, Caceres, Fig. 1). The site is characterized by a mean annual temperature of 16^{o}C, mean annual precipitation of ca. 700 mm, falling mostly from November until May, and by a very dry summer. Similar to most Mediterranean grasland, grazing (<0.7 cows ha^{-1}) is the main land use in the site. The site is defined as a typical Mediterranean savanna ecosystem, low density of oak trees (mostly *Quercus Ilex* (L.), ~20 trees ha^{-1}) dominated by a herbaceous stratum. The experiment itself was restricted to an open grassland area which was not influenced by tree canopy. The herbaceous stratum is dominated by species of the three main functional plant forms (grasses, forbs and legumes). The fraction of the three plant forms varied seasonally according to their phenological status (Table 1). Overall, leaf area measurements of the herbaceous stratum characterized the growing season phenology as peaking early in April and achieving senescence by the end of May (Table 1).

The experiment consisted of four randomized blocks of about 20 m x 20 m. Each block was separated into four plots of 9 m x 9 m with a buffer of 2 m in between to avoid boundary effects. In each block, four treatments were applied (see Fig. 1):

(a) control treatment (C) with no fertilization;

(b) Nitrogen addition treatment (+N) with an application of 100 kg N ha^{-1} as potassium nitrate (KNO_3) and ammonium nitrate (NH_4NO_3);

(c) Phosphorous addition treatment (+P) with an application of 50 kg P ha^{-1} as monopotassium phosphate (KH_2PO_4); and

(d) N and P addition treatment (+NP), juxtaposing treatments (b) and (c).

Each fertilizer was dissolved in water and sprayed on foliage early in the growing season (March 21st, 2014). The same amount of water used in the fertilizer solutions (~ 2 L m^{-2}) was sprayed on the C treatment to avoid water imbalances among treatments.

Within each plot, two permanent, non-disturbed parcels (32 in total, see black squares in Fig 1) were dedicated to monitor CO_2 fluxes (net ecosystem CO_2 exchange, NEE; and daytime ecosystem respiration, R_{eco}). While NEE measurements were performed over the course of the day (from early in the morning to late afternoon), spectral measurements were conducted simultaneously with flux measurements only around noon on half of the parcels (16 in total).

Flux and spectral measurements were carried out in four field campaigns:

- Campaign #1: before fertilization (March 20th, 2014),
- Campaign #2: three weeks after fertilization (April 15th, 2014) during the peak of the growing period,
- Campaigns #3 and #4: on May 7th and 27th, 2014, respectively, concurring with the drying period were performed to evaluate joint effects related to physiological senescence processes.

Ancillary measurements were taken in every field campaign as follows: green plant area index (PAI_g) and aboveground biomass were directly measured by harvest in four parcels (0.25m x

196 0.25m) within each plot in the area surrounding that where spectral and flux measurements
197 were taken. All samples were refrigerated just after collection, and transported for laboratory
198 analyses. Fresh samples were separated into functional groups, the sample was scanned and
199 green plant area was measured using image analysis (WinRHIZO, Regent Instruments Inc.,
200 Canada). Afterwards, fresh samples were dried in an oven at 65 °C for 48 hours and weighed
201 to determine dry biomass. To analyze the nutrient content in leaf mass, biomass subsamples
202 were ground in a ball mill (RETSCH MM200, Retsch, Haan, Germany) and total C and N
203 concentrations were determined with an elemental analyzer (Vario EL, Elementar, Hanau,
204 Germany). P concentrations were also measured: 100-mg biomass subsamples were diluted in
205 3 ml of HNO_3 65%, (Merck, Darmstadt, Germany) and microwave digested at high pressure
206 (Multiwave, Anton Paar, Graz, Austria; Raessler et al. (2005). Afterwards, elemental analysis
207 was conducted using inductively coupled plasma - optical emission spectrometry (ICP-OES,
208 Optima 3300 DV, Perkin Elmer, Norwalk, USA).
209
210 **2.2 Flux measurements and Meteorological data**
211 Net CO_2 fluxes were measured with three transparent chambers of a closed dynamic system.
212 The chambers consisted of a cubic (0.6m x0.6m x0.6 m) transparent low-density polyethylene
213 structure connected to an infrared gas analyzer (IRGA LI-840, Lincoln, NE, USA), which
214 measures CO_2 and water vapor mole fractions (W) at 1 Hz. The chambers were equipped with
215 different sensors to acquire environmental and soil variables, all installed at the chamber
216 ceiling: Photosynthetically Active Radiation (*PAR)* was measured with a quantum sensor (Li-
217 190, Li-Cor, Lincoln, NE, USA) placed outside of the chamber to be handled and leveled; air
218 and vegetation temperatures were measured with a thermistor probe (T_a, type 107, Campbell
219 Scientific, Logan, Utah, USA) and an infrared thermometer (T_c, IRTS-P, Apogee, UT, USA);
220 atmospheric pressure (P) was measured inside the chamber using a barometric pressure sensor

(CS100, Campbell Scientific, Logan, Utah, USA). The chambers were also equipped with soil temperature and humidity sensors; soil water content was determined with an impedance soil moisture probe (Theta Probe ML2x, Delta-T Devices, Cambridge, UK) at 5 cm depth and soil temperature (type 107, Campbell Scientific, Logan, Utah, USA) at 10 cm depth. Vapor pressure deficit (VPD) was computed using T_c and relative humidity, which was derived from water vapor molar fraction measured with the IRGA.

The chamber operated as a closed dynamic system. A small pump circulates an air flow of 1 L min^{-1} through the sample circuit: air is drawn from inside the chamber - through three porous-hanging tubes spatially distributed through the chamber headspace - to the infrared gas analyzer; this air flow is then returned to the chamber. The hanging tubes allowed spatially distributed sampling, obviating the need to homogenize air during chamber deployment. Nevertheless, one small fan (12V, 0.14A) was fixed at 0.3 m on a floor corner of the chamber and angled 45º upward.

A 0.6x0.6m metal collar was installed in each permanent parcel of each plot. The collar provided a flat surface onto which the bottom of the chamber was placed. The chamber was open and ventilated during 1 min prior to measurement, so that initial air composition and temperature in the confined environment of the chamber represented natural atmospheric conditions (as much NEE as Reco). For the NEE measurement, the transparent chamber was placed on the collar (closed position, lasted 3 minutes as a general rule), and fluxes were calculated from the rate of change of the CO_2 molar fraction (referenced to dry air) within the chamber. Similar procedure was carried out for R_{eco} but using an opaque blanket that covered the entire chamber and kept it dark during the measurements (PAR values around 0). Fluxes were calculated according to Pérez-Priego et al. (2015).

Shortly, the flux calculation algorithm reduces flux uncertainties by including the change-point detection method to determine the stabilization time, which defines the initial slope of

the regressions, and a bootstrap resampling-based method to improve confidence in regression parameters and to optimize the number of data points used for flux calculation. In addition, a statistical analysis of residuals was performed to automatically detect the best fit among alternative regressions (i.e. quadratic, hyperbolic tangent saturating function, exponential, linear). These analyses were implemented in a self-developed R Package (available upon authors request or at the following link http://r-forge.r-project.org/projects/respchamberproc/). NEE and R_{eco} measurements were taken over the course of the day (from sunrise to sunset) for each field campaign. Chamber disturbance effects and correction for systematic and random errors (i.e. leakage, water dilution and gas density correction, and light attenuation by the chamber wall) were applied according to Perez-Priego et al., (2015).

2.3 Field spectral measurements

Midday spectral measurements at canopy level were carried out under clear sky conditions using two portable spectrometers (HR4000, OceanOptics, USA) characterized by different spectral resolutions. Spectrometer 1, characterized by a Full Width at Half Maximum (FWHM) of 0.1 nm and a 700-800 nm spectral range was specifically designed for the estimation of sun-induced chlorophyll fluorescence at the O_2-A band (760 nm). Spectrometer 2 (FWHM = 1 nm, 400 - 1000 nm spectral range) was used for the computation of reflectance and vegetation indices. Spectrometers were housed in a thermally regulated Peltier box, keeping the internal temperature at 25°C in order to reduce dark current drift. The spectrometers were spectrally calibrated with a source of known characteristics (CAL-2000 mercury argon lamp, OceanOptics, USA) while the radiometric calibration was inferred from cross-calibration measurements performed with a calibrated FieldSpec FR Pro spectrometer (ASD, USA). This spectrometer was calibrated by the manufacturer with yearly frequency.

Incident solar irradiance was measured by nadir observations of a leveled calibrated standard reflectance panel (Spectralon; LabSphere, USA). Measurements were acquired using bare fiber optics with an angular field of view of 25°. The average canopy plane was observed from nadir at a distance of 110 cm (43 cm diameter field of view) allowing for collecting measurements of 50% of the surface area covered by the chamber measurements. The manual rotation of a mast mounted horizontally on the tripod allowed sequential observation of the vegetated target and the white reference calibrated panel. More in detail, every acquisition session consisted in the consecutive collection of the following spectra: instrument dark current, radiance of the white reference panel, canopy radiance and radiance of the white reference panel. The radiance of the reference panel at the time of the canopy measurement was then estimated by linear interpolation.

For every acquisition, 3 and 10 scans (for Spectrometers 1 and 2, respectively) were averaged and stored as a single file. Five measurements were collected for each plot. Spectral data were acquired with dedicated software (Meroni and Colombo, 2009) and processed with a specifically developed IDL (ITTVIS IDL 7.1.1) application. This application allowed the basic processing steps of raw data necessary for the computation of the hemispherical conical reflectance factor described by Meroni et al. (2011).

The following indices were selected as suitable to investigate long term nutrient-mediated effects on photosynthesis. The NDVI (Rouse et al., 1974) was selected because it correlates well with plant area and among traditional spectral vegetation indices is used worldwide by classical LUE models as a surrogate for *f*APAR (Di Bella et al., 2004). The MTCI (Dash and Curran, 2004) was selected because it was specifically designed for canopy chlorophyll content estimation, and recently used as proxy for *f*APAR as well as NDVI. In this study we used the PRI and SIF as surrogates for LUE. A scaled PRI (sPRI) calculated as (PRI+1)/2 was

used. SIF was estimated by exploiting the spectral fitting method described in Meroni et al. (2010), assuming linear variation of the reflectance and fluorescence in the O_2-A absorption band region. The spectral interval used for SIF estimation was set to 759.00 - 767.76 nm for a total of 439 spectral channels used. For methodological distinction among existing approaches, hereafter SIF is referred to as F760. Because F760 is affected by PAR we use the apparent chlorophyll fluorescence yield (Fy760; Rossini et al., 2010) computed as the ratio between F760 and the incident radiance in a nearby spectral region. A summary of the formulation to compute the vegetation indices and their corresponding target and proxy in the LUE model approach are presented in Table 2.

2.4 Relationship between GPP and remote sensing data

Ecosystem-level GPP was computed as the difference between NEE and daytime R_{eco} taken consecutively with the chambers. To assess how GPP is modulated by light among treatments and over the phenological cycle of the herbaceous stratum, we computed the parameters of photosynthetic light response curve (PLRC). Specifically, the Michaelis–Menten function was fitted to GPP and PAR data taken throughout the course of the day (from sunrise until sunset) for each field campaign and treatment as follows:

$$GPP_i = \frac{\alpha \times \beta \times PAR_i}{\beta + PAR_i \times \alpha}, \quad [1]$$

where α is a parameter describing the photosynthetic quantum yield (μmol CO_2 μmol photons^{-1}), and β is the parameter that extrapolates to GPP at saturating light condition (μmol CO_2 m^{-2} s^{-1}). According to Ruimy et al. (1994), we used the optimized parameters of the PLRC as defined in Eq. (1) to estimate the GPP at 2000 μmol quantum m^{-2} s^{-1} of PAR (hereafter referred to GPP_{2000}).

We evaluated direct relationships between those GPP measurements taken around noon (between 11:00 and 15:00 pm solar time) with the chamber (GPP_{noon}) and sequentially measurements of Fy760 and spectral indices (NDVI, sPRI, MTCI). In addition, to avoid confounding factors in the relationship between Fy760 and sPRI and photosynthesis, we also used GPP_{2000} as a maximum photosynthetic capacity descriptor.

2.5 Monteith's light-use efficiency modelling approaches

Following Monteith's LUE framework (Eq. 2) two alternative modeling approaches were used:

$$GPP = LUE \times fAPAR \times PAR, \quad [2]$$

i. ***Meteo-driven methods (MM);*** based on the MOD17 formulation, fAPAR is approached through the relationship with NDVI and includes limiting functions f(meteo), which are based on climatic driving parameters to limit maximum LUE (LUE_{max}). Alternatively, Eq. (2) was reformulated as follows:

$$GPP = LUE_{max} \times f(meteo) \times (a_0 \times NDVI + a_1) \times PAR, \quad [3]$$

where LUE_{max}, a_o, and a_1 are model parameters. Three different f(meteo) functions were tried;

a) **MM-VPD,** this method is a simplification of the original MOD17, in which *f*(meteo) includes two linear ramp functions of both maximum and minimum vapour pressure deficit (VPD) and minimum temperature (T). Since minimum temperature was not limiting at the site, we fixed the *f*(meteo) parameters as suggested by Heinsch et al. (2006) but constraining only a function based on VPD as follows:

$$f(meteo) = \left[1 - \left(\frac{VPD - VPD_{min}}{VPD_{max} - VPD_{min}}\right)\right], \quad [4]$$

then, VPD_{max} and VPD_{min} are defined as the three parameters of the *f(meteo)* term.

b) **MM-SWC**, where *f*(meteo) includes a soil water content (SWC) function (Migliavacca et al., 2011) as the limiting factor of LUE_{max}:

$$f(meteo) = \frac{1}{1+exp^{(SWC_{max}-a\times SWC)}}, \quad [5]$$

here, SWC_{max} and *a* are defined as the parameters of the *f(meteo)* term.

c) **MM (SWC-VPD)**, where *f*(meteo) includes both soil water content and VPD functions as limiting factors:

$$f(meteo) = \left[1 - \left(\frac{VPD-VPD_{min}}{VPD_{max}-VPD_{min}}\right)\right] \times \left[\frac{1}{1+exp^{(SWC_{max}-a\times SWC)}}\right], \quad [6]$$

here, VPD_{max}, VPD_{min}, SWC_{max} and *a* are defined as the parameters of the *f(meteo)* term.

ii. ***RS-based method (RSM)****;* based on a solution of Eq.(1) as follows:

$$GPP = LUE \times fPAR \times PAR = (a_0 \times Ph + a_1) \times (a_2 \times St + a_3) \times PAR$$

$$= (b_0 \times Ph + b_1 \times St + b_2 \times Ph \times St + b_3) \times PAR, \quad [7]$$

where four alternative model formulations were obtained from the combination of the sPRI or Fy760 as the physiological related proxy (*Ph*) for LUE, and NDVI or MTCI as structural-related (*St*) proxy for *f*APAR. In Eq. 7, b_0, b_1, b_2, and b_3 are fitting parameters (Rossini et al., 2010).

2.5 Statistical analysis and model performance

All model formulations were optimized using GPP_{noon} and spectral measurements taken at midday. Since the means of spectral measurements per treatment could have unequal variance, a Welch's t-test was performed to evaluate significant differences between the mean values of the different vegetation indices for each treatment and over the four field campaigns. In addition, an analysis of covariance (ANCOVA) was used to test whether or not there was a

significant interaction by the treatment effect between GPP_{noon} and Fy760 and different spectral indices. Like vegetation indices, a t-test was performed to the daily average of GPP taken over the course of the day (GPP_{daily}).

2.5.1 Cross-validation analyses and model evaluation

Different model formulations were evaluated in leave-one-out (loo) cross-validation: from the whole dataset composed by *n* observations, one data point at a time was removed. The model was fitted against the $n-1$ remaining data points (training set) while the excluded data (validation set) were used for model evaluation. The cross-validation process was then repeated *n* times, with each of the *n* observations used exactly once as the validation set. For each validation set of the cross-validated model, statistics were calculated.

Model accuracy was evaluated by means of different statistics according to Janssen and Heuberger (1995): root mean square error (RMSE), relative root mean square error (rRMSE) determination coefficient (r^2) and model efficiency (ME). The model performances in loo cross-validation were also calculated and reported as $RMSE_{cv}$, $rRMSE_{cv}$, r^2cv and ME_{cv}.

The Akaike Information Criterion (AIC_{cv}) was used to evaluate the trade-off between model complexity (i.e. number of parameters) and explanatory power (i.e. goodness-of-fit) of the different model formulations proposed. The AIC_{cv} is a method based on information theory that is useful for statistical and empirical model selection purposes (Akaike, 1998). Following Anderson et al. (2000), in this analysis we used the following definition of AIC_{cv}:

$$AIC_{cv} = 2(\rho + 1) + n\left[ln\left(\frac{RSS_{cv}}{n}\right)\right] \quad [8]$$

where *n* is the number of samples (i.e. observations), *p* is the number of model parameters and RSS_{cv} is the residual sum of squares divided by n.

384 The LUE model formulations proposed in Section 2.4 can be ranked according to AIC_{cv},
385 where the model with lowest AIC_{cv} is considered the best among the different model
386 formulations.
387 All model parameters (MM, and RSM) were estimated by using a Gauss-Newton nonlinear
388 least square optimization method (Bates and Watts, 2008), and standard errors of parameters
389 were estimated by bootstrapping (number of sampling, n = 500; Efron and Tibshirani (1994)),
390 both implemented in the R standard package (R version 3.0.2, R Development Core Team,
391 2011).
392

393 **3. Results**

394 **3.1 Effects of fertilization on plant nutrient contents and GPP**

395 Fertilization caused strong variations in leaf N and P content among treatments, plant
396 forms and across field campaigns (Table 2); while total N content in plants ranged slightly
397 between 13.8±1.2 and 15.4±1.7 mg g^{-1} for the C and +P treatments over the whole
398 experiment, the largest increases in total N content were found in the peak of the growing
399 season (#2, March 20th, 2014), when +NP and +N treatments reached values of up to 23.7±2.0
400 and 23.5±4.1 mg g^{-1}, respectively. Although slightly lower, the differences in total N content
401 between C and +P, and +NP and +N remained high over the drying period. Total P content
402 was higher in +NP and +P treatments after fertilization, as compared to +N and C treatments.
403 Consequently, the N:P ratio at the first campaign after fertilization (#2) achieved values of up
404 to 14.2, 6.6, 6, and 3.7, in +N, C, +NP, and +P treatments, respectively. Similar differences in
405 N:P between treatments were also observed during the drying period (#3 and #4, Table 2). On
406 the other hand, PAI_g ranged from 0.4 m^2 m^{-2} in campaign #4 to up to 2.5 m^2 m^{-2} in campaign
407 #2. No differences were found in PAI_g among treatments since grazing apparently offset any

potential difference in the green aboveground production. Regarding variations in the fraction of plant forms, no significant differences were found between treatments.

Fertilization caused significant differences in the GPP_{daily} ($p<0.05$) between N-addition treatments (mean values of 19.62±4.15 and 18.19±5.67 $\mu molCO_2\ m^{-2}\ s^{-1}$ for +N and +NP, respectively) and C and +P treatments (14.31±5.39 and 14.40±4.09 $\mu molCO_2\ m^{-2}\ s^{-1}$, respectively) in the peak of the growing season (campaign #2); a relative difference of 37% in GPP_{daily} values was found between +N and +NP and C treatments. During the drying period, however, GPP was substantially down regulated (campaigns #3 and #4) and no significant differences were found in GPP_{daily}, regardless of differences in plant N content observed among treatments. The potential photosynthetic capacity GPP_{2000} (Fig 2) derived from PLRC was similar in the four treatments in the pretreatment period (campaign #1, Fig 2a). GPP_{2000} varied throughout the season and peaked in the campaign #2 (April 15th) in all treatments. At this time PLRC of the +N and +NP treatments diverged clearly from no N addition treatments (C and +P, Fig 2b). GPP_{2000} was higher in +N and +NP treatments (18.6 and 20.1$\mu mol\ CO_2\ m^{-2}\ s^{-1}$, respectively) compared to C and +P treatments (14.9 and 15.4 $\mu mol\ CO_2\ m^{-2}\ s^{-1}$, respectively). After campaign #2, when the soil layer at 5 cm depth dried out appreciably (volumetric water content achieved values of 3% vol., data not shown), vegetation progressively senesced and GPP_{2000} in turn was down-regulated and converged to similar values in all treatments, regardless the higher N content observed in +N and +NP treatments as compared with C and +P treatments (Table 1). During the drying season, GPP_{2000} decreased in all treatments ranging between 5.6 and 8 $\mu molCO_2\ m^{-2}\ s^{-1}$ and no differences among treatments was observed (Fig 2 c and d). These results indicate that the senescence of the herbaceous stratum, which is regulated by water availability, strongly modulated the photosynthetic capacity of the vegetation over the season.

3.2 – Effects of fertilization on remote sensing data

Optical properties of the analyzed plots were similar during campaign #1, before the nutrient application. A pronounced seasonal time course was observed for both *Ph* (sPRI and Fy760) and structural indices (*St*; NDVI and MTCI) with maximum values during the second campaign. It is interesting to note that while for *St* indices the maximum values were reached in +N plots, +NP plots showed maximum *Ph* values. Vegetation indices and Fy760 then decreased in the drying period (Figure 3). As for GPP, differences between treatments were more evident during campaign #2 when C plots showed statistically lower values for all the indices considered, while only MTCI was able to detect significant differences between N fertilized plots (+N and +NP). Furthermore significant differences in Fy760 and MTCI between C and the other three treatments were found ($p<0.05$) in the drying period (campaign #4,). NDVI varied significantly with changes in PAI_g with values of 0.4 in the campaign #4 up to 0.8 in the campaign #2 ($p<0.001$, $r^2=0.79$).

3.3 Relationship between remote sensing data and GPP

While *Ph* indices (Fy760 and sPRI) varied linearly with GPP_{noon} in all treatments ($p<0.001$, $r^2=0.66$ for Fy760 and $p<0.001$, $r^2=0.79$ for sPRI, respectively, Fig 4 a and b,), different patterns were observed for *St*: NDVI and GPP were best fitted by an exponential regression ($p<0.001$, $r^2=0.77$ Fig 4 c), while a weak linear relationship between MTCI and GPP_{noon} ($p<0.05$, $r^2=0.45$, Fig 4 d) was found. Although a weak relation between MTCI and GPP_{noon} was found, MTCI was strongly correlated with plant N content ($y=14.17x-2.49$, $p<0.001$, $r^2=0.86$). Note that these results are computed excluding data taken in the pre-treatment campaign (#1) and differences in the relationship between remote sensing data and GPP_{noon} among treatments can be only attributed to nutrient-induced effects. The ANCOVA

457 test did not show significant differences neither in slope nor intercept of the relationship
458 between GPP_{noon} and sPRI, and NDVI across treatments. However, barely significant
459 differences were found in the relationship between GPP_{noon} and Fy760 ($p<0.1$, Fig 4b) and
460 significant between GPP_{noon} and MTCI ($p<0.01$, Fig 4d) between N addition treatments (+N
461 and +NP) and C treatments (C and +P).

462 Similar to GPP_{noon}, GPP_{2000} was also significantly related to mean midday sPRI
463 ($r^2=0.76$, $p<0.001$, Fig. 5a) and Fy760 ($r^2=0.76$, $p<0.001$, Fig. 5b). As expected, an
464 exponential regression fitted best for NDVI, while a poor relationship with MTCI was found
465 (data not shown).

466

467 **3.4 Modeling GPP**

468 Based on the AIC_{cv} criterion, MM (VPD- SWC) outperformed MM-VPD, MM-SWC
469 and RSM models. Although MM (VPD-SWC) showed high accuracy in the predictions
470 ($ME_{cv}=0.879$, $r^2_{cv}=0.881$), this model had a tendency to underestimate observation at high
471 GPP_{noon} values (see comparison between model predictions and observations, Figures 6a-6c).
472 Note that the highest biases in modeled GPP_{noon} values among MM models belong to +N and
473 +NP treatments in field campaign #2. Since the four treatments experienced the same
474 environmental conditions (i.e. comparable values of SWC, VPD, air temperature), this bias
475 can be attributed to the higher N content (+N and +NP treatments) as compared to C and +P
476 treatments. Remarkably, residuals of the MM (VPD-SWC) taken from periods with moist soil
477 (SWC>15) were significantly correlated with sPRI and Fy760 ($p<0.05$, Fig. 7 a and b,
478 respectively). However, no biases between residuals and predictions were observed in RSM
479 over the span of values and treatments (Fig. 8). Results from the evaluation of model
480 performance indicated that RSM performs best when NDVI rather than MTCI, is used as *St* in

481 the Eq.7 and, hence, as a proxy for *f*APAR (Table 3). Our results indicated that RSM
482 performs best when either *Ph* (sPRI or Fy760) is combined with NDVI as *St*.

483

484 **4. Discussion**

485 **4.1 Effects of nutrients on GPP and remote sensing data and their relationships**

486 Nutrient fertilization, particularly N inputs, induced physiological changes manifested as an
487 increase in photosynthetic capacity under high light conditions (Fig. 2; Hirose and Werger
488 (1994). As we expected, plant N content showed to be a trait of photosynthesis that influences
489 a variety of aspects of photosynthetic physiology (Ciompi et al., 1996; Sugiharto et al., 1990).
490 These physiological changes were reflected on the optical properties, particularly on
491 fluorescence and sPRI. The increase in fluorescence with N fertilization inputs was recently
492 explained as the combined effect that a higher N content has on 1) chlorophyll content, which
493 magnifies APAR and enhances fluorescence signal, and on 2) the increased photosynthetic
494 capacity that results in reduced NPQ activity and consequently increases the fluorescence
495 signal (Cendrero-Mateo et al., 2015).The relationships between GPP_{noon} and Fy760 is not
496 unique and may vary from optimal to non-optimal environmental conditions (i.e. nutrient
497 deficiencies, water stress), when other regulatory mechanisms might reduce the degree of
498 coupling between fluorescence and photosynthesis (Cendrero-Mateo et al., 2015; Porcar-
499 Castell et al., 2012). Although Fy760 was positively correlated with GPP_{noon}, barely
500 significant differences in the slope of this relationship were observed between treatments (Fig.
501 4 b). Further studies are needed to fully explore the relationship between Fy760 and GPP_{noon}
502 under different stress conditions and over different ecosystems. However, if confirmed, the
503 effect of nutrient availability on the relationship between Fy760 and GPP_{noon} could have
504 important implications in GPP modeling. This result suggests that the inclusion of a

correction factor related to leaves N:P stoichiometry should be considered when modeling GPP assuming a linear relationship with fluorescence at plant functional type level (Guanter et al., 2014; Joiner et al., 2013).

In this study we also explored the capability of remote sensing to describe ecosystem functional properties defined as those quantities that summarize and integrate ecosystem processes and responses to environmental conditions and can be retrieved from ecosystem level fluxes (e.g. GPP_{2000}) and structural measurements (Reichstein et al., 2014). GPP at light saturation (i.e. GPP_{2000}) is one example of an ecosystem functional property, shown here to be quite correlated to sPRI and Fy760 (Fig. 5). This result suggests that sPRI and Fy760 open also new opportunities for remote sensing products to describe the spatiotemporal variability of essential descriptors of ecosystem functioning (Musavi et al., 2015). Inferring GPP_{2000} using remote-sensing has important implication both for monitoring global carbon cycle and for benchmarking terrestrial biosphere models.

MTCI was tightly related with N content (r^2=0.86, p<0.001), independent of other structural variables (i.e. PAI_g), and can be used as a good indicator of N availability. Although MTCI has been proven to be very sensitive to variations in chlorophyll contents (Dash and Curran, 2004) and hence linkable with light absorption processes, it was weakly correlated with GPP, particularly in plots added with N (+N and +NP; r^2=0.27, p<0.01, Fig 4 d). A quite wide range of GPP_{noon} values were found at high values of MTCI – high GPP_{noon} values corresponding to the growing season and low ones to the drying period – which can be explained by two simultaneous mechanisms.

First, despite the high plant N content, physiological mechanisms including stomatal control or reduced carboxylation efficiency down-regulate GPP (Huang et al., 2004) and ultimately might break the relationship between GPP_{noon} and MTCI. Second, MTCI tracks changes in N

content regardless changes in canopy structure occuring during the dry season when grass achieved senescence (i.e. green to dry biomass ratio, PAI_g). More studies aimed at the separation of the combined effects of N and changes in green/dry biomass fractions on *f*APAR are essential. On the other hand, although NDVI followed the seasonal dynamic of PAIg, it saturated at high GPP_{noon} values indicating the low ability of this index to detect spatial variations induced by N fertilization.

Although optical measurements were taken at high spatial resolution (<0.36 m^2), the separation of confounding factors affecting sPRI or Fy760 is essential to elucidate the mechanistic association between sPRI or Fy760 and GPP. Like sPRI, the retrieval of Fy760 from the apparent reflectance signal can be also affected by vegetation structure or canopy background components (Zarco-Tejada et al., 2013). After optimization and selection of the best model parameters using NDVI and sPRI (or Fy760) as driver, we analyzed the response of simulated GPP to variations in NDVI and sPRI (or Fy760, Fig 9). Results indicate that at high GPP levels, Fy760 and sPRI but less NDVI shaped GPP. However, at low GPP levels, either Fy760 or sPRI responded to GPP on a small scale (Fig 9b). Figure 9 suggests that the relationship between NDVI and sPRI or Fy760 is not unique and NDVI may play an important role in driving GPP in ecosystem characterized by marked seasonal variations. Our results highlight the complementarity between NDVI and Fy760 or sPRI. Particularly, NDVI assisted Fy760 or sPRI in predicting GPP under conditions with low biomass (i.e. low LAI), when confounding factors may affect Fy760 or sPRI. In semi-arid ecosystems, the lack of sensitivity of sPRI or Fy760 to changes in GPP during dry conditions have been explained by the soil background effect on the reflectance signal (Barton and North, 2001; Mänd et al., 2010; Zarco-Tejada et al., 2013). Accordingly, Rahman et al., (2004) pointed out that conditions where sPRI performs best are in dense canopies with low portion of bare soil.

554 **4.2 Performances of different LUE modeling approaches.**

555 Here we aim at answering the question how can we better simulate GPP using LUE modeling
556 with varying nutrient availability and environmental conditions by drawing comparisons
557 between the two model philosophies; RSM against MM approaches. There are an increasing
558 number of studies focused on the development of LUE models driven by remotely sensed
559 information to better explain spatio-temporal variations of GPP (Gitelson et al., 2014; Rossini
560 et al., 2012; Rossini et al., 2014). However, nutrient availability (and in particular N) greatly
561 influence the spatial variability of LUE even within the same plant-functional type (e.g.
562 grasslands) and further studies are essential. The slightly better performance in cross
563 validation of the MM (VPD-SWC) against all model configurations, including RSM, supports
564 the importance of a joint use of SWC and VPD as key parameters to constraint LUE in arid
565 and semi-arid ecosystems (Prince and Goward, 1995). However, residual analyses
566 demonstrated that MM (VPD-SWC) was unable to track N-induced differences in GPP during
567 the growing period, when both parameters are not limiting (Fig. 7). By contrast, accurate
568 estimates of GPP were obtained with RSM both over the drying and the growing periods.
569 These results also indicate the importance of physiological descriptors to constrain LUE,
570 which prevails over structural factors controlling *f*APAR (i.e. green biomass) under given
571 environmental conditions and encourage the use of hyperspectral remote sensing for
572 diagnostic upscaling of GPP.

573 With sPRI or Fy760 as a proxy for LUE, RSM is presented as a valuable means to diagnose
574 N-induced effects on physiology. Our results show the limits of MM in predicting the spatial
575 and temporal variability of GPP when LUE is not controlled by meteorological drivers alone
576 (VPD, temperature, soil moisture)**.** Accordingly, GPP is eventually biased whenever neither
577 climatic nor structural state variables explicitly reveal spatial changes in the LUE parameter
578 associated with plant nutrient availability; residuals showed a clear tendency to underestimate

579 the highest modeled GPP values, significantly correlated to Fy760 and sPRI (Fig.7). From a
580 practical point of view, the forcing variables of RSM approaches may show a better
581 observational coverage. In effect, the satellite-based retrievals of RSM forcing variables could
582 additionally overcome representativeness limitations and potential regional or seasonal biases
583 in meteorological fields (Dee et al., 2011). The uncertainties in forcing variables of MM (i.e.
584 temperature, VPD and soil moisture) could propagate and affects the GPP estimates.

585

586 **5. Concluding remarks**

587 1. Fy760 and sPRI correlated well with GPP: both increased with N content and
588 decreased with senescence.
589 2. MTCI can be used as a good descriptor of N content in plants but the
590 relationship with GPP breaks down under drought conditions.
591 3. Meteo-driven models were able to describe temporal variations in GPP, and
592 soil moisture can be a key parameter to better track the seasonal dynamics of
593 LUE in arid environments. However, meteo-driven models were unable to
594 describe N-induced effects on GPP. Important implication can be derived from
595 these results and uncertainties in the prediction of global GPP still remain
596 when meteo-driven models do not account for plant nutrient availability.
597 4. sPRI or Fy760 provide valuable means to diagnose nutrient-induced effects on
598 the photosynthetic activity and, therefore, should be included in diagnostic
599 GPP models.

600

Author contribution

OPP, MM, and MRo conceived the analyses, wrote the introduction, results and discussion, and led the preparation and revision of the manuscript; FF, TJ made hyperspectral measurements, computed spectral indices and fluorescence, and wrote part of the methods section; JH, MS and OPP made chamber measurements, soil and vegetation lab analysis and wrote part of the methods section; JH organized the dataset; OK provided technical assistance in the design and construction of the chambers and data acquisition system and wrote part of the methods section; GM and AC designed the fertilization protocol, organized sampling, provided technical assistance for the managing of the experiment and contributed to data interpretation; TW and OPP developed the R package for flux calculations, computed GPP and flux uncertainties and contributed to statistical analyses and interpretation. NC and MRe contributed to analyses and interpretation and to draft the manuscript. All authors discussed the results and contributed to the manuscript.

Acknowledgements

The authors acknowledge the Alexander von Humboldt Foundation and the Max Planck Research Award that is funding the research activity. We acknowledge City council of Majadas de Tietar for its support. The authors acknowledge Andrea Perez-Bargueno, and Enrique Juarez-Alcalde from (University of Extreamdura), Ramon Lopez-Jimenez (CEAM), Kathrin Henkel, and Martin Hertel from (MPI-Jena) and Marco Celesti (UNIMIB) for the support in the field, lab analysis and the development of the transparent chambers; Javier Pacheco Labrador and Maria Pilar Isabel Martin (CSIC) for help calibrating the radiometric system. We thank Professor Andrew S. Kowalski (University of Granada, Spain) for his review of the manuscript and constructive comments.

Figure Captions

Fig 1. Overview of the experimental site (SMANIE): the experimental blocks are drawn on an image acquired with the hyperspectral AHS (Sensytech Inc., Beverly, MA, USA) sensor during April 2014.

Fig 2. Photosynthetic light response curves derived for each growing period: (a) pretreatment and (b) post-treatment and drying periods (c and d). Treatments are presented in different colors. Lines represent the Michaelis–Menten function fitting gross photosynthesis (GPP, $\mu molCO_2 m^{-2} s^{-1}$) and photosynthetic active radiation (PAR, $\mu molm^{-2} s^{-1}$).

Fig 3. Seasonal time course of mean midday physiologically-driven vegetation indices; (a) scale photochemical reflectance index, sPRI (b) apparent fluorescence yield (Fy760), and structure-driven vegetation indices, (c) NDVI, and (d) MTCI among C, +N, +NP and +P treatments in a Mediterranean grassland in Spain. Bars indicate standard deviation, N = 4. Different letters denote significant dierence between treatments (Weilch t test, $P < 0.05$).

Fig 4. Relationship between GPP and remote sensing data: (a) scaled photochemical reflectance index (sPRI), (b) apparent fluorescence yield, (c) normalized difference vegetation index (NDVI), and (d) MTCI. Square symbols represent measurements taken in the pre-treatment (#1) and circles after fertilization (#2–#4). Data were obtained at midday and lines represent results from the regressions for each treatment excluding measurements in the pre-treatment.

Fig 5. Relationship between GPP2000 and average values of sPRI and (b) apparent fluorescence yield (Fy760). Lines represent results the best linear regressions fitting the data.

Fig 6. Comparison between measured GPP and GPP modeled with the best performing LUE model for each kind of formulation: MM (VPD, panel a), MM (SWC, panel b), MM (including VPD and SWC, panel c), RSM (sPRI-NDVI panel d), and RSM (Fy760-NDVI, panel e). Results from the cross-validation analysis are presented in Table 3.

Fig 7. Correlation between residuals of the MM (VPD-SWC) model and (a) scaled photochemical reflectance index (sPRI) and (b) chlorophyll fluorescence yield (Fy760) taken from periods with high soil water content (SWC>15%, red circles). No correlation was observed when SWC<15% ($p>0.5$, black circles).

Fig 8. Plot between residuals of both the Meteo-driven model (MM-VPD) and Remote Sensing-based method (RSM) and modeled GPP values. Both lines represent the local polynomial regression fitting of the residuals against predicted values.

Fig 9. Contour plot indicating how variation in photosynthesis (GPP, $\mu mol\ CO_2\ m^{-2}\ s^{-1}$) are explained by variations in the LUE and fPAR parameters of the RSM. While (a) sPRI and (b) Fy760 are indistinctly used as a proxy of LUE, the NDVI is taken as *f*PAR.

Table Captions

673 **Table 1.** Ancillary data resulting from the analysis. Green Plant Area Index (PAIg), fraction
674 of PAI in different plant forms (fPAI), and C, N, and P plant content. The N:P ratio also is
675 shown. Data correspond to the mean value and standard deviation (SD) of the subsamples
676 taken in each plot and treatment.
677
678 **Table 2.** Spectral vegetation indices computed in this study. Vegetation indices are classified
679 into two major classes based on their suitability in inferring fAPAR (structural related
680 indices) and LUE (physiologically-related indices) parameters. R denotes the reflectance at
681 the specified wavelength (nm). NDVI: normalized difference vegetation index; MTCI:
682 MERIS terrestrial chlorophyll index; NDI: normalized difference index; sPRI: scaled
683 Photochemical Reflectance Index; Fy760: apparent fluorescence yield at 760 nm.
684
685 **Table 3.** Results from the model evaluation one leave out cross-validation analysis across
686 LUE model configurations and vegetation indices. Based on AICcv, the best performance
687 among formulation test for each method is highlighted text bold.
688
689 **Table 4. Abbreviations.**

References

Akaike, H.: Information Theory and an Extension of the Maximum Likelihood Principle. In: Selected Papers of Hirotugu Akaike, Parzen, E., Tanabe, K., and Kitagawa, G. (Eds.), Springer Series in Statistics, Springer New York, 1998.

Anderson, D. R., Burnham, K. P., and Thompson, W. L.: Null Hypothesis Testing: Problems, Prevalence, and an Alternative, The Journal of Wildlife Management, 64, 912-923, 2000.

Baret, F., Houlès, V., and Guérif, M.: Quantification of plant stress using remote sensing observations and crop models: The case of nitrogen management, Journal of Experimental Botany, 58, 869-880, 2007.

Barton, C. V. M. and North, P. R. J.: Remote sensing of canopy light use efficiency using the photochemical reflectance index: Model and sensitivity analysis, Remote Sensing of Environment, 78, 264-273, 2001.

Bates, D. M. and Watts, D. G.: Frontmatter. In: Nonlinear Regression Analysis and Its Applications, John Wiley & Sons, Inc., 2008.

Campbell, P. K. E., Middleton, E. M., Corp, L. A., and Kim, M. S.: Contribution of chlorophyll fluorescence to the apparent vegetation reflectance, Science of The Total Environment, 404, 433-439, 2008.

Cendrero-Mateo, M. P., Carmo-Silva, A. E., Porcar-Castell, A., Hamerlynck, E. P., Papuga, S. A., and Moran, M. S.: Dynamic response of plant chlorophyll fluorescence to light, water and nutrient availability, Functional Plant Biology, doi: http://dx.doi.org/10.1071/FP15002, 2015. -, 2015.

Ciompi, S., Gentili, E., Guidi, L., and Soldatini, G. F.: The effect of nitrogen deficiency on leaf gas exchange and chlorophyll fluorescence parameters in sunflower, Plant Science, 118, 177-184, 1996.

Damm, A., Elbers, J., Erler, A., Gioli, B., Hamdi, K., Hutjes, R., Kosvancova, M., Meroni, M., Miglietta, F., Moersch, A., Moreno, J., Schickling, A., Sonnenschein, R., Udelhoven, T., van der Linden, S., Hostert, P., and Rascher, U.: Remote sensing of sun-induced fluorescence to improve modeling of diurnal courses of gross primary production (GPP), Global Change Biology, 16, 171-186, 2010.

Dash, J. and Curran, P. J.: The MERIS terrestrial chlorophyll index, International Journal of Remote Sensing, 25, 5403-5413, 2004.

Dee, D. P., Uppala, S. M., Simmons, A. J., Berrisford, P., Poli, P., Kobayashi, S., Andrae, U., Balmaseda, M. A., Balsamo, G., Bauer, P., Bechtold, P., Beljaars, A. C. M., van de Berg, L., Bidlot, J., Bormann, N., Delsol, C., Dragani, R., Fuentes, M., Geer, A. J., Haimberger, L., Healy, S. B., Hersbach, H., Hólm, E. V., Isaksen, L., Kållberg, P., Köhler, M., Matricardi, M., McNally, A. P., Monge-Sanz, B. M., Morcrette, J. J., Park, B. K., Peubey, C., de Rosnay, P., Tavolato, C., Thépaut, J. N., and Vitart, F.: The ERA-Interim reanalysis: configuration and performance of the data assimilation system, Quarterly Journal of the Royal Meteorological Society, 137, 553-597, 2011.

Di Bella, C. M., Paruelo, J. M., Becerra, J. E., Bacour, C., and Baret, F.: Effect of senescent leaves on NDVI-based estimates of fAPAR: Experimental and modelling evidences, International Journal of Remote Sensing, 25, 5415-5427, 2004.

Drolet, G. G., Middleton, E. M., Huemmrich, K. F., Hall, F. G., Amiro, B. D., Barr, A. G., Black, T. A., McCaughey, J. H., and Margolis, H. A.: Regional mapping of gross light-use efficiency using MODIS spectral indices, Remote Sensing of Environment, 112, 3064-3078, 2008.

Efron, B. and Tibshirani, R. J.: An Introduction to the Bootstrap. Chapman & Hall/CRC Monographs on Statistics & Applied Probability, 1994.

738 Filella, I., Porcar-Castell, A., Munné-Bosch, S., Bäck, J., Garbulsky, M. F., and Peñuelas, J.:
739 PRI assessment of long-term changes in carotenoids/chlorophyll ratio and short-term changes
740 in de-epoxidation state of the xanthophyll cycle, International Journal of Remote Sensing, 30,
741 4443-4455, 2009.
742 Flexas, J., Escalona, J. M., Evain, S., Gulías, J., Moya, I., Osmond, C. B., and Medrano, H.:
743 Steady-state chlorophyll fluorescence (Fs) measurements as a tool to follow variations of net
744 CO2 assimilation and stomatal conductance during water-stress in C3 plants, Physiologia
745 Plantarum, 114, 231-240, 2002.
746 Frankenberg, C., O'Dell, C., Berry, J., Guanter, L., Joiner, J., Köhler, P., Pollock, R., and
747 Taylor, T. E.: Prospects for chlorophyll fluorescence remote sensing from the Orbiting
748 Carbon Observatory-2, Remote Sensing of Environment, 147, 1-12, 2014.
749 Gamon, J. A., Peñuelas, J., and Field, C. B.: A narrow-waveband spectral index that tracks
750 diurnal changes in photosynthetic efficiency, Remote Sensing of Environment, 41, 35-44,
751 1992.
752 Gamon, J. A., Serrano, L., and Surfus, J. S.: The photochemical reflectance index: an optical
753 indicator of photosynthetic radiation use efficiency across species, functional types, and
754 nutrient levels, Oecologia, 112, 492-501, 1997.
755 Garbulsky, M. F., Peñuelas, J., Gamon, J., Inoue, Y., and Filella, I.: The photochemical
756 reflectance index (PRI) and the remote sensing of leaf, canopy and ecosystem radiation use
757 efficiencies: A review and meta-analysis, Remote Sensing of Environment, 115, 281-297,
758 2011.
759 Gelybó, G., Barcza, Z., Kern, A., and Kljun, N.: Effect of spatial heterogeneity on the
760 validation of remote sensing based GPP estimations, Agricultural and Forest Meteorology,
761 174–175, 43-53, 2013.
762 Gitelson, A. A., Peng, Y., Arkebauer, T. J., and Schepers, J.: Relationships between gross
763 primary production, green LAI, and canopy chlorophyll content in maize: Implications for
764 remote sensing of primary production, Remote Sensing of Environment, 144, 65-72, 2014.
765 Grace, J., Nichol, C., Disney, M., Lewis, P., Quaife, T., and Bowyer, P.: Can we measure
766 terrestrial photosynthesis from space directly, using spectral reflectance and fluorescence?,
767 Global Change Biology, 13, 1484-1497, 2007.
768 Guanter, L., Rossini, M., Colombo, R., Meroni, M., Frankenberg, C., Lee, J.-E., and Joiner,
769 J.: Using field spectroscopy to assess the potential of statistical approaches for the retrieval of
770 sun-induced chlorophyll fluorescence from ground and space, Remote Sensing of
771 Environment, 133, 52-61, 2013.
772 Guanter, L., Zhang, Y., Jung, M., Joiner, J., Voigt, M., Berry, J. A., Frankenberg, C., Huete,
773 A. R., Zarco-Tejada, P., Lee, J.-E., Moran, M. S., Ponce-Campos, G., Beer, C., Camps-Valls,
774 G., Buchmann, N., Gianelle, D., Klumpp, K., Cescatti, A., Baker, J. M., and Griffis, T. J.:
775 Global and time-resolved monitoring of crop photosynthesis with chlorophyll fluorescence,
776 Proceedings of the National Academy of Sciences, 111, E1327-E1333, 2014.
777 Hall, F. G., Hilker, T., Coops, N. C., Lyapustin, A., Huemmrich, K. F., Middleton, E.,
778 Margolis, H., Drolet, G., and Black, T. A.: Multi-angle remote sensing of forest light use
779 efficiency by observing PRI variation with canopy shadow fraction, Remote Sensing of
780 Environment, 112, 3201-3211, 2008.
781 Heinsch, F. A., Maosheng, Z., Running, S. W., Kimball, J. S., Nemani, R. R., Davis, K. J.,
782 Bolstad, P. V., Cook, B. D., Desai, A. R., Ricciuto, D. M., Law, B. E., Oechel, W. C.,
783 Hyojung, K., Hongyan, L., Wofsy, S. C., Dunn, A. L., Munger, J. W., Baldocchi, D. D.,
784 Liukang, X., Hollinger, D. Y., Richardson, A. D., Stoy, P. C., Siqueira, M. B. S., Monson, R.
785 K., Burns, S. P., and Flanagan, L. B.: Evaluation of remote sensing based terrestrial
786 productivity from MODIS using regional tower eddy flux network observations, Geoscience
787 and Remote Sensing, IEEE Transactions on, 44, 1908-1925, 2006.

788 Hilker, T., Coops, N. C., Hall, F. G., Black, T. A., Wulder, M. A., Nesic, Z., and Krishnan, P.:
789 Separating physiologically and directionally induced changes in PRI using BRDF models,
790 Remote Sensing of Environment, 112, 2777-2788, 2008.
791 Hirose, T. and Werger, M. J. A.: Photosynthetic capacity and nitrogen partitioning among
792 species in the canopy of a herbaceous plant community, Oecologia, 100, 203-212, 1994.
793 Huang, Z. A., Jiang, D. A., Yang, Y., Sun, J. W., and Jin, S. H.: Effects of Nitrogen
794 Deficiency on Gas Exchange, Chlorophyll Fluorescence, and Antioxidant Enzymes in Leaves
795 of Rice Plants, Photosynthetica, 42, 357-364, 2004.
796 Janssen, P. H. M. and Heuberger, P. S. C.: Calibration of process-oriented models, Ecological
797 Modelling, 83, 55-66, 1995.
798 Joiner, J., Guanter, L., Lindstrot, R., Voigt, M., Vasilkov, A. P., Middleton, E. M.,
799 Huemmrich, K. F., Yoshida, Y., and Frankenberg, C.: Global monitoring of terrestrial
800 chlorophyll fluorescence from moderate-spectral-resolution near-infrared satellite
801 measurements: methodology, simulations, and application to GOME-2, Atmos. Meas. Tech.,
802 6, 2803-2823, 2013.
803 Krause, G. H. and Weis, E.: Chlorophyll fluorescence as a tool in plant physiology,
804 Photosynth Res, 5, 139-157, 1984.
805 Lee, J.-E., Frankenberg, C., van der Tol, C., Berry, J. A., Guanter, L., Boyce, C. K., Fisher, J.
806 B., Morrow, E., Worden, J. R., Asefi, S., Badgley, G., and Saatchi, S.: Forest productivity and
807 water stress in Amazonia: observations from GOSAT chlorophyll fluorescence, 2013.
808 Madani, N., Kimball, J. S., Affleck, D. L. R., Kattge, J., Graham, J., van Bodegom, P. M.,
809 Reich, P. B., and Running, S. W.: Improving ecosystem productivity modeling through
810 spatially explicit estimation of optimal light use efficiency, Journal of Geophysical Research:
811 Biogeosciences, 119, 2014JG002709, 2014.
812 Mänd, P., Hallik, L., Peñuelas, J., Nilson, T., Duce, P., Emmett, B. A., Beier, C., Estiarte, M.,
813 Garadnai, J., Kalapos, T., Schmidt, I. K., Kovács-Láng, E., Prieto, P., Tietema, A.,
814 Westerveld, J. W., and Kull, O.: Responses of the reflectance indices PRI and NDVI to
815 experimental warming and drought in European shrublands along a north–south climatic
816 gradient, Remote Sensing of Environment, 114, 626-636, 2010.
817 McMurtrey, J. E., Middleton, E. M., Corp, L. A., Campbell, P., Butcher, L. M., and Daughtry,
818 C. S. T.: Optical reflectance and fluorescence for detecting nitrogen needs in Zea mays L, 21-
819 25 July 2003 2003, 4602-4604 vol.4607.
820 Meroni, M., Barducci, A., Cogliati, S., Castagnoli, F., Rossini, M., Busetto, L., Migliavacca,
821 M., Cremonese, E., Galvagno, M., Colombo, R., and di Cella, U. M.: The hyperspectral
822 irradiometer, a new instrument for long-term and unattended field spectroscopy
823 measurements, Review of Scientific Instruments, 82, -, 2011.
824 Meroni, M., Busetto, L., Colombo, R., Guanter, L., Moreno, J., and Verhoef, W.:
825 Performance of Spectral Fitting Methods for vegetation fluorescence quantification, Remote
826 Sensing of Environment, 114, 363-374, 2010.
827 Meroni, M. and Colombo, R.: 3S: A novel program for field spectroscopy, Computers &
828 Geosciences, 35, 1491-1496, 2009.
829 Migliavacca, M., Galvagno, M., Cremonese, E., Rossini, M., Meroni, M., Sonnentag, O.,
830 Cogliati, S., Manca, G., Diotri, F., Busetto, L., Cescatti, A., Colombo, R., Fava, F., Morra di
831 Cella, U., Pari, E., Siniscalco, C., and Richardson, A. D.: Using digital repeat photography
832 and eddy covariance data to model grassland phenology and photosynthetic CO2 uptake,
833 Agricultural and Forest Meteorology, 151, 1325-1337, 2011.
834 Monteith, J. L.: Solar Radiation and Productivity in Tropical Ecosystems, Journal of Applied
835 Ecology, 9, 747-766, 1972.
836 Musavi, T., Mahecha, M. D., Migliavacca, M., Reichstein, M., van de Weg, M. J., van
837 Bodegom, P. M., Bahn, M., Wirth, C., Reich, P. B., Schrodt, F., and Kattge, J.: The imprint of

838 plants on ecosystem functioning: A data-driven approach, International Journal of Applied
839 Earth Observation and Geoinformation, 43, 119-131, 2015.
840 Nichol, C. J., Huemmrich, K. F., Black, T. A., Jarvis, P. G., Walthall, C. L., Grace, J., and
841 Hall, F. G.: Remote sensing of photosynthetic-light-use efficiency of boreal forest,
842 Agricultural and Forest Meteorology, 101, 131-142, 2000.
843 Parazoo, N. C., Bowman, K., Fisher, J. B., Frankenberg, C., Jones, D. B. A., Cescatti, A.,
844 Pérez-Priego, Ó., Wohlfahrt, G., and Montagnani, L.: Terrestrial gross primary production
845 inferred from satellite fluorescence and vegetation models, Global Change Biology, 20, 3103-
846 3121, 2014.
847 Peñuelas, J., Garbulsky, M. F., and Filella, I.: Photochemical reflectance index (PRI) and
848 remote sensing of plant CO2 uptake, New Phytologist, 191, 596-599, 2011.
849 Peñuelas, J., Poulter, B., Sardans, J., Ciais, P., van der Velde, M., Bopp, L., Boucher, O.,
850 Godderis, Y., Hinsinger, P., Llusia, J., Nardin, E., Vicca, S., Obersteiner, M., and Janssens, I.
851 A.: Human-induced nitrogen–phosphorus imbalances alter natural and managed ecosystems
852 across the globe, Nat Commun, 4, 2013.
853 Pérez-Priego, O., López-Ballesteros, A., Sánchez-Cañete, E., Serrano-Ortiz, P., Kutzbach, L.,
854 Domingo, F., Eugster, W., and Kowalski, A.: Analysing uncertainties in the calculation of
855 fluxes using whole-plant chambers: random and systematic errors, Plant and Soil, doi:
856 10.1007/s11104-015-2481-x, 2015. 1-16, 2015.
857 Pérez-Priego, O., Zarco-Tejada, P. J., Miller, J. R., Sepulcre-Cantó, G., and Fereres, E.:
858 Detection of water stress in orchard trees with a high-resolution spectrometer through
859 chlorophyll fluorescence In-Filling of the O 2-A band, IEEE Transactions on Geoscience and
860 Remote Sensing, 43, 2860-2868, 2005.
861 Porcar-Castell, A., Garcia-Plazaola, J., Nichol, C., Kolari, P., Olascoaga, B., Kuusinen, N.,
862 Fernández-Marín, B., Pulkkinen, M., Juurola, E., and Nikinmaa, E.: Physiology of the
863 seasonal relationship between the photochemical reflectance index and photosynthetic light
864 use efficiency, Oecologia, 170, 313-323, 2012.
865 Porcar-Castell, A., Mac Arthur, A., Rossini, M., Eklundh, L., Pacheco-Labrador, J.,
866 Anderson, K., Balzarolo, M., Martín, M. P., Jin, H., Tomelleri, E., Cerasoli, S., Sakowska, K.,
867 Hueni, A., Julitta, T., Nichol, C. J., and Vescovo, L.: EUROSPEC: at the interface between
868 remote sensing and ecosystem CO2 flux measurements in Europe, Biogeosciences Discuss.,
869 12, 13069-13121, 2015.
870 Prince, S. D. and Goward, S. N.: Global Primary Production: A Remote Sensing Approach,
871 Journal of Biogeography, 22, 815-835, 1995.
872 Raessler, M., Rothe, J., and Hilke, I.: Accurate determination of Cd, Cr, Cu and Ni in
873 woodlice and their skins—is moulting a means of detoxification?, Science of The Total
874 Environment, 337, 83-90, 2005.
875 Rahman, A. F., Cordova, V. D., Gamon, J. A., Schmid, H. P., and Sims, D. A.: Potential of
876 MODIS ocean bands for estimating CO2 flux from terrestrial vegetation: A novel approach,
877 Geophysical Research Letters, 31, L10503, 2004.
878 Reichstein, M., Bahn, M., Mahecha, M. D., Kattge, J., and Baldocchi, D. D.: Linking plant
879 and ecosystem functional biogeography, Proceedings of the National Academy of Sciences,
880 111, 13697-13702, 2014.
881 Rossini, M., Cogliati, S., Meroni, M., Migliavacca, M., Galvagno, M., Busetto, L.,
882 Cremonese, E., Julitta, T., Siniscalco, C., di Cella, U. M., and Colombo, R.: Remote sensing-
883 based estimation of gross primary production in a subalpine grassland, Biogeosciences, 9,
884 2565-2584, 2012.
885 Rossini, M., Meroni, M., Migliavacca, M., Manca, G., Cogliati, S., Busetto, L., Picchi, V.,
886 Cescatti, A., Seufert, G., and Colombo, R.: High resolution field spectroscopy measurements

for estimating gross ecosystem production in a rice field, Agricultural and Forest Meteorology, 150, 1283-1296, 2010.
Rossini, M., Migliavacca, M., Galvagno, M., Meroni, M., Cogliati, S., Cremonese, E., Fava, F., Gitelson, A., Julitta, T., Morra di Cella, U., Siniscalco, C., and Colombo, R.: Remote estimation of grassland gross primary production during extreme meteorological seasons, International Journal of Applied Earth Observation and Geoinformation, 29, 1-10, 2014.
Rossini, M., Nedbal, L., Guanter, L., Ač, A., Alonso, L., Burkart, A., Cogliati, S., Colombo, R., Damm, A., Drusch, M., Hanus, J., Janoutova, R., Julitta, T., Kokkalis, P., Moreno, J., Novotny, J., Panigada, C., Pinto, F., Schickling, A., Schüttemeyer, D., Zemek, F., and Rascher, U.: Red and far red Sun-induced chlorophyll fluorescence as a measure of plant photosynthesis, Geophysical Research Letters, 42, 1632-1639, 2015.
Rouse, J. W., Haas, R. H., Schell, J. A., Deering, D. W., and Harlan, J. C.: Monitoring the vernal advancements and retro gradation of natural vegetation, Greenbelt, MD, USA., 1974. 1974.
Ruimy, A., Saugier, B., and Dedieu, G.: Methodology for the estimation of terrestrial net primary production from remotely sensed data, Journal of Geophysical Research, 99, 5263 - 5283, 1994.
Schlemmer, M., Gitelson, A., Schepers, J., Ferguson, R., Peng, Y., Shanahan, J., and Rundquist, D.: Remote estimation of nitrogen and chlorophyll contents in maize at leaf and canopy levels, International Journal of Applied Earth Observation and Geoinformation, 25, 47-54, 2013.
Suárez, L., Zarco-Tejada, P. J., Sepulcre-Cantó, G., Pérez-Priego, O., Miller, J. R., Jiménez-Muñoz, J. C., and Sobrino, J.: Assessing canopy PRI for water stress detection with diurnal airborne imagery, Remote Sensing of Environment, 112, 560-575, 2008.
Sugiharto, B., Miyata, K., Nakamoto, H., Sasakawa, H., and Sugiyama, T.: Regulation of Expression of Carbon-Assimilating Enzymes by Nitrogen in Maize Leaf, Plant Physiology, 92, 963-969, 1990.
Tremblay, N., Wang, Z., and Cerovic, Z.: Sensing crop nitrogen status with fluorescence indicators. A review, Agron. Sustain. Dev., 32, 451-464, 2012.
Walker, A. P., Beckerman, A. P., Gu, L., Kattge, J., Cernusak, L. A., Domingues, T. F., Scales, J. C., Wohlfahrt, G., Wullschleger, S. D., and Woodward, F. I.: The relationship of leaf photosynthetic traits – Vcmax and Jmax – to leaf nitrogen, leaf phosphorus, and specific leaf area: a meta-analysis and modeling study, Ecology and Evolution, 4, 3218-3235, 2014.
Wang, W., Yao, X., Yao, X., Tian, Y., Liu, X., Ni, J., Cao, W., and Zhu, Y.: Estimating leaf nitrogen concentration with three-band vegetation indices in rice and wheat, Field Crops Research, 129, 90-98, 2012.
Yuan, W., Cai, W., Liu, S., Dong, W., Chen, J., Arain, M. A., Blanken, P. D., Cescatti, A., Wohlfahrt, G., Georgiadis, T., Genesio, L., Gianelle, D., Grelle, A., Kiely, G., Knohl, A., Liu, D., Marek, M. V., Merbold, L., Montagnani, L., Panferov, O., Peltoniemi, M., Rambal, S., Raschi, A., Varlagin, A., and Xia, J.: Vegetation-specific model parameters are not required for estimating gross primary production, Ecological Modelling, 292, 1-10, 2014.
Zarco-Tejada, P. J., Suarez, L., and Gonzalez-Dugo, V.: Spatial Resolution Effects on Chlorophyll Fluorescence Retrieval in a Heterogeneous Canopy Using Hyperspectral Imagery and Radiative Transfer Simulation, Geoscience and Remote Sensing Letters, IEEE, 10, 937-941, 2013.

Campaign	Treatment	Total PAIg (m^2 m^{-2})	Total PAIg (m^2 m^{-2})	Forbs f_{PAI}	Grass f_{PAI}	legumes f_{PAI}	Total C content (mg g^{-1})	Total C content (mg g^{-1})	Total N content (mg g^{-1})	Total N content (mg g^{-1})	Total P content (mg g^{-1})	Total P content (mg g^{-1})	N/P (mg g^{-1})
Date	--	mean	SD	%	%	%	mean	SD	mean	SD	mean	SD	--
#1 March 20 th, 2014 Growing period Pre-treatment	C	0.85	0.18	35.5	56.8	7.7	425	--	17.7	--	2.08	--	8.5
	N	0.76	0.21	39.2	45.1	15.0	463	--	18.6	--	1.99	--	9.34
	NP	1.03	0.30	29.1	54.3	12.9	421	--	18.1	--	1.90	--	9.52
	P	0.95	0.21	26.6	66.6	6.9	369	--	16.9	--	1.94	--	8.71
#2 April 15 th, 2014 Growing period Post-treatment	C	2.02	0.43	14.5	85.2	0.3	413	152	14.6	0.8	2.23	0.02	6.6
	N	2.17	0.91	11.9	87.6	0.4	384	121	23.7	2.0	1.68	0.03	14.2
	NP	2.46	0.45	4.1	95.6	0.3	377	330	23.5	4.1	3.95	0.04	6.0
	P	1.66	0.58	14.2	85.7	0.1	394	212	15.4	1.7	4.22	0.06	3.7
#3 May 7 th, 2014 Dry period	C	1.08	0.27	43.0	55.1	1.9	447	52	14.2	1.3	2.41	0.02	5.9
	N	1.29	0.58	28.3	70.7	1.0	449	114	20.1	3.1	1.86	0.03	10.8
	NP	0.84	0.21	27.2	71.8	1.0	438	64	20.6	1.2	3.50	0.04	5.9
	P	1.37	0.57	39.5	58.5	2.0	444	206	14.7	0.8	3.83	0.03	3.8
#4 May 27 th, 2014 Dry period	C	0.44	0.10	66.7	33.3	0.0	442	2	13.8	1.2	2.12	0.01	6.5
	N	0.48	0.28	36.4	63.6	0.0	448	3	19.0	2.8	1.93	0.02	9.8
	NP	0.53	0.26	40.6	59.4	0.0	442	1	18.5	3.4	2.63	0.02	7.1
	P	0.71	0.31	56.1	43.9	0.0	441	72	13.2	0.7	2.62	0.02	5.0

Table 1. Ancillary data resulting from the analysis. Green Plant Area Index (PAIg), fraction of PAI in different plant forms (fPAI), and C, N, and P plant content. The N:P ratio also is shown. Data correspond to the mean value and standard deviation (SD) of the subsamples taken in each plot and treatment.

Index	Target	Model proxy	Formulation	References
NDVI	*Green biomass & Leaf area*	f_{APAR}	$(R_{800}-R_{680})/(R_{800}+R_{680})$	Rouse et al., 1974
MTCI	*Chlorophyll & Nitrogen content*	f_{APAR}	$(R_{754} - R_{709})/(R_{709} - R_{681})$	Dash and Curran, 2004
sPRI	Physiology	LUE	$(R_{531}-R_{570})/(R_{531}+R_{570})$	Gamon et al., 1992
Fy_{760}	Physiology	LUE	Chlorophyll Fluorescence In-Filling of the O_2-A Band	Meroni and Colombo, 2006

Table 2. Spectral vegetation indices computed in this study. Vegetation indices are classified into two major classes based on their suitability in inferring fAPAR (structural related indices) and LUE (physiologically-related indices) parameters. R denotes the reflectance at the specified wavelength (nm). NDVI: normalized difference vegetation index; MTCI: MERIS terrestrial chlorophyll index; NDI: normalized difference index; sPRI: scaled Photochemical Reflectance Index; Fy760: apparent fluorescence yield at 760 nm.

LUE Model	Variable	RMSE	rRMSE	r2	ME	RMSEcv	rRMSEcv	r2cv	MEcv	AICcv
MM-VPD	NDVI	3.041	23.439	0.894	0.802	3.143	24.671	0.877	0.788	160.887
MM-SWC	NDVI	2.663	32.909	0.849	0.848	2.769	34.840	0.835	0.829	148.417
MM (VPD-SWC)	**NDVI**	**2.230**	**21.727**	**0.894**	**0.893**	**2.357**	**23.266**	**0.881**	**0.879**	**127.478**
RSM	**PRI-NDVI**	**2.390**	**24.112**	**0.879**	**0.877**	**2.760**	**30.832**	**0.844**	**0.837**	**140.627**
RSM	PRI-MTCI	3.113	35.793	0.794	0.792	3.489	42.123	0.751	0.739	171.125
RSM	**Fy760-NDVI**	**2.490**	**27.743**	**0.868**	**0.867**	**2.835**	**34.242**	**0.834**	**0.828**	**144.116**
RSM	Fy760-MTCI	3.676	46.770	0.710	0.710	4.074	52.224	0.654	0.644	191.275

Table 3. Results from the model evaluation one leave out cross validation analysis across LUE model configurations and vegetation indices. Based on AICcv, the best performance among formulation test for each method is highlighted text bold.

Table 4. List of abbreviations

a, **a_o**, and **a_1** are model parameters; **b_0**, **b_1**, **b_2**, and **b_3** are fitting parameters of RSM; **EFPs**, ecosystem functional properties; ***f*(meteo),** limiting functions relying on meteorologically-driven data; ***f*APAR**, fraction of absorbed photosynthetically active radiation; ***f*PAIg**, fraction of *PAIg* in different plant forms; **Fy760**, sun-induced chlorophyll Fluorescence yield at 760 nm; **GPP**, gross primary productivity; **GPP_{noon}**: instantaneous gross photosynthetic rate taken at solar noon (between 11:00 and 15:00 pm solar time); GPP_{daily}: mean value of the diurnal time course of gross photosynthetic rate; **GPP_{2000}**, gross primary productivity estimated at 2000 of PAR; **LUE,** light use-efficiency; **LUE_m** potential or maximum LUE; **MM**, meteorologically driven model; **MM-VPD,** simplifier model of the original MOD17 that account for VPD in *f*(meteo); **MM(SWC-VPD)** meteorologically-driven model that account for VPD and soil moisture in *f*(meteo); **MTCI**, MERIS terrestrial-chlorophyll index; **NDVI**, Normalized difference vegetation index; **NEE**, net ecosystem CO_2 exchange; **PAIg**, Green Plant Area Index; **PAR**, Photosynthetically active radiation; ***ph***, physiologically-related parameter of RSM referring to either sPRI or Fy760 as a proxy for LUE; **PLRC**, photosynthetic light response curve; **PRI**, photochemical reflectance index; **R_{eco}**, daytime ecosystem respiration; **RSM**, remote sensing based models; **SIF**, sun-induced chlorophyll fluorescence; **sPRI**, scaled-photochemical reflectance index; ***st***, structurally-related parameter of RSM referring to either NDVI or MTCI as a proxy for *f*APAR; **SWC**, soil water content; **SWC_{max}** parameter of the *f(meteo)* term; **VPD**, vapor pressure deficit; **VPD_{max}** and **VPD_{min}** are fitting parameters of the *f(meteo)* term; $\boldsymbol{\alpha}$ is a parameter describing the photosynthetic quantum yield; $\boldsymbol{\beta}$ is the parameter that extrapolates to GPP at saturating light condition.

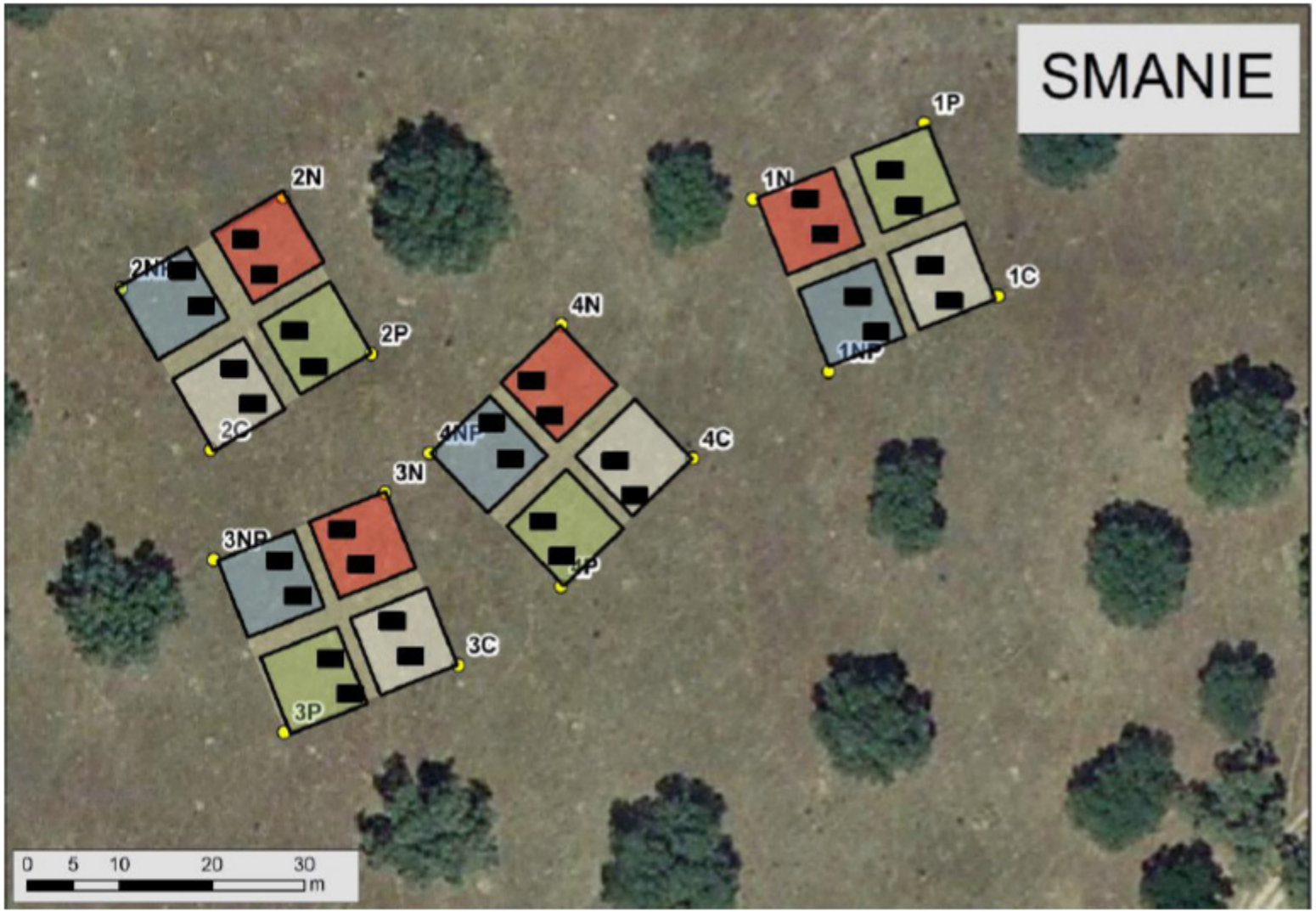

Fig. 1

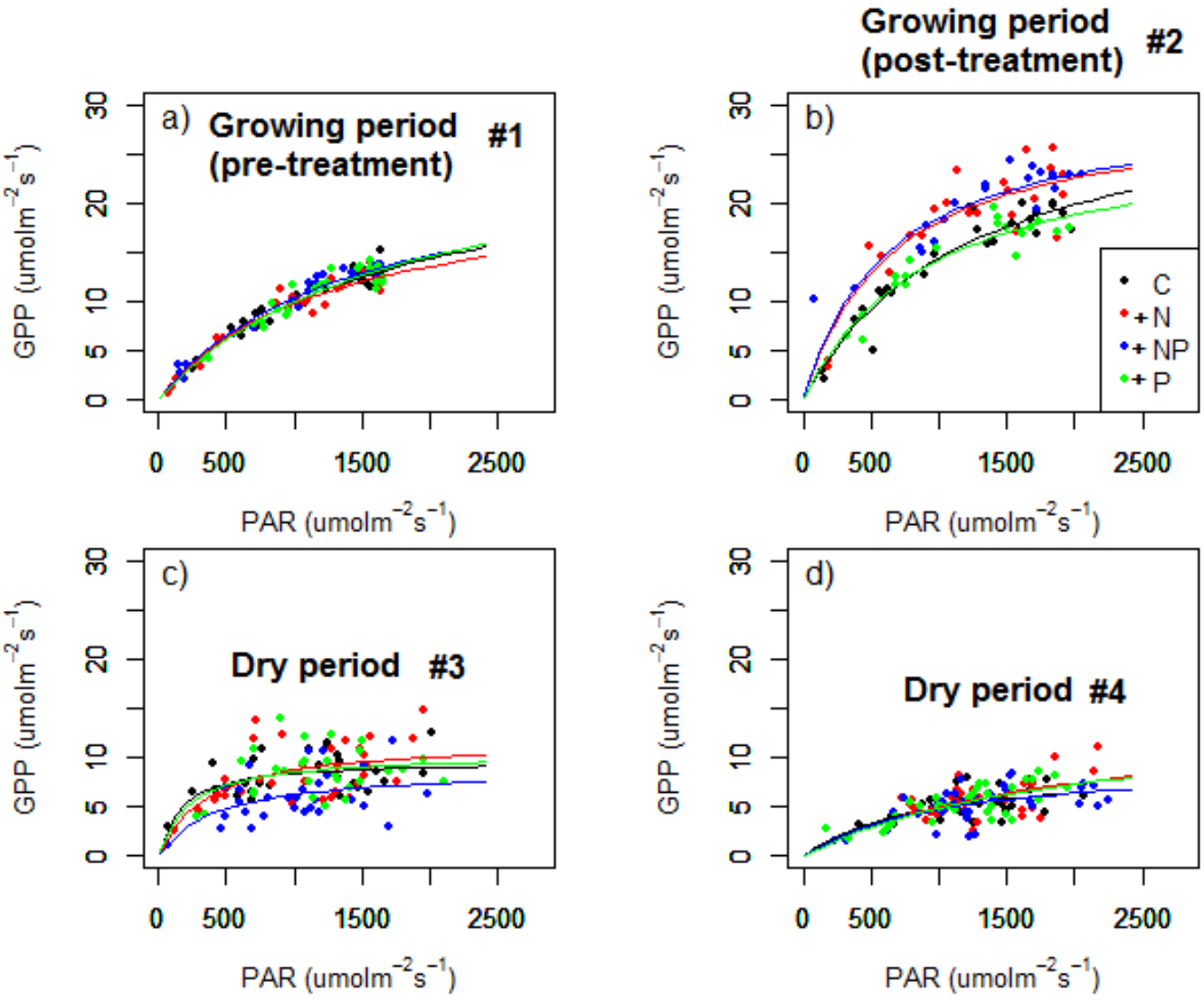
a)
Growing period
(pre-treatment)
#1
b)
Growing period
(post-treatment)
#2
c)
Dry period
#3
d)
Dry period
#4
C
+ N
+ NP
+ P
GPP (umolm^{-2}s^{-1})
PAR (umolm^{-2}s^{-1})
0
5
10
20
30
500
1500
2500

Fig. 2

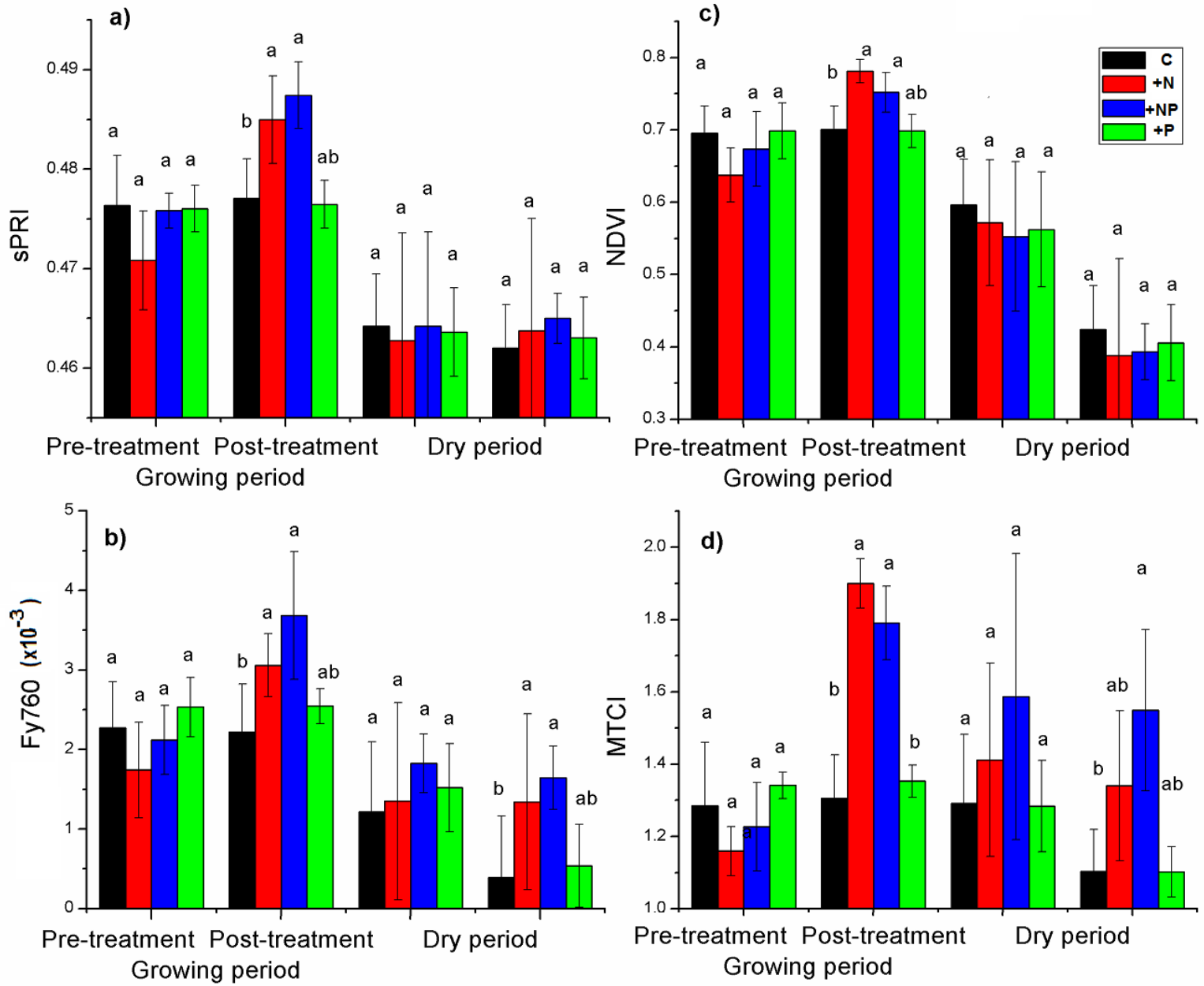
a)
sPRI
0.49
0.48
0.47
0.46
Pre-treatment
Post-treatment
Dry period
Growing period
c)
NDVI
0.8
0.7
0.6
0.5
0.4
0.3
C
+N
+NP
+P
b)
Fy760 (x10-3)
5
4
3
2
1
0
d)
MTCI
2.0
1.8
1.6
1.4
1.2
1.0

Fig. 3

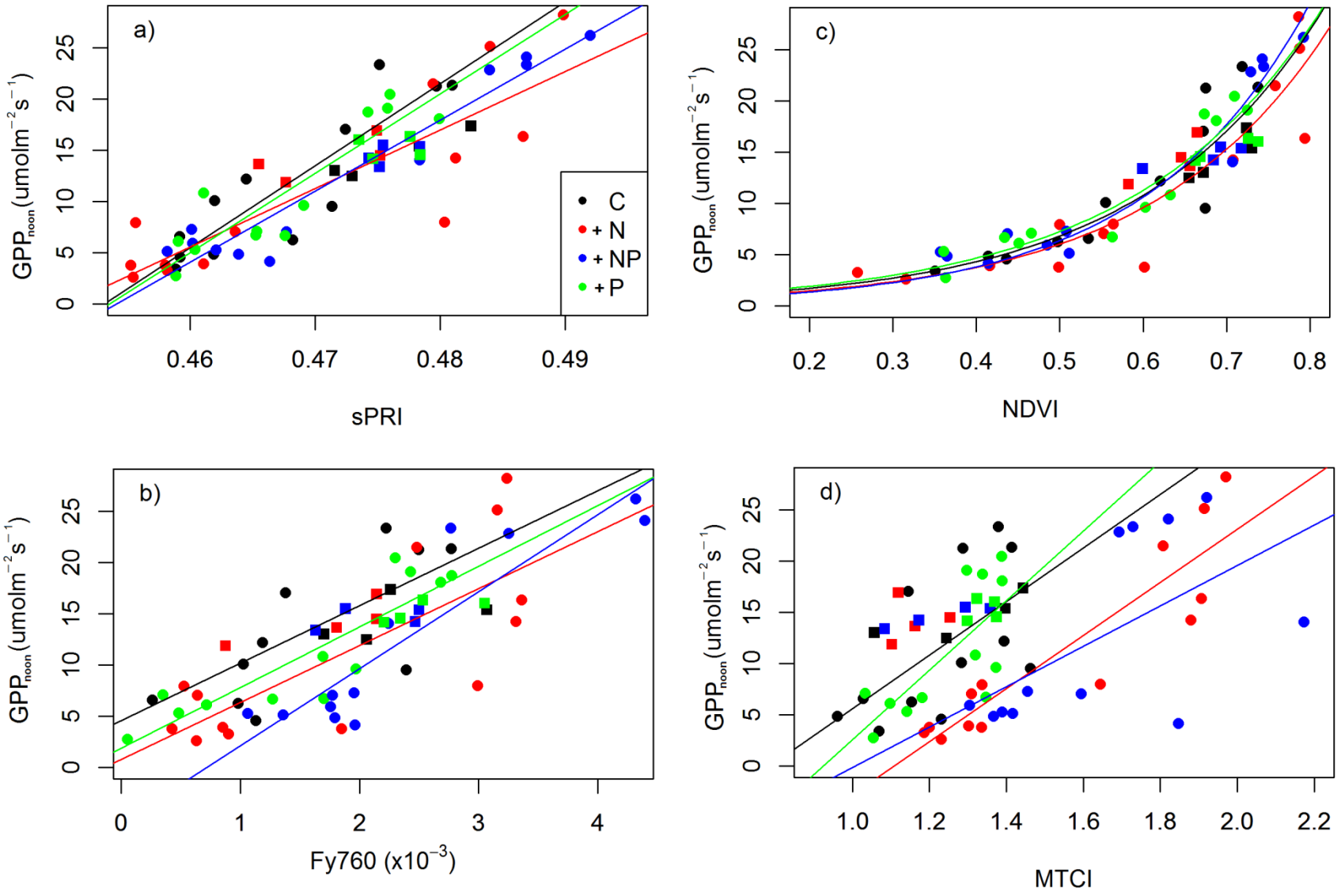

Fig. 4

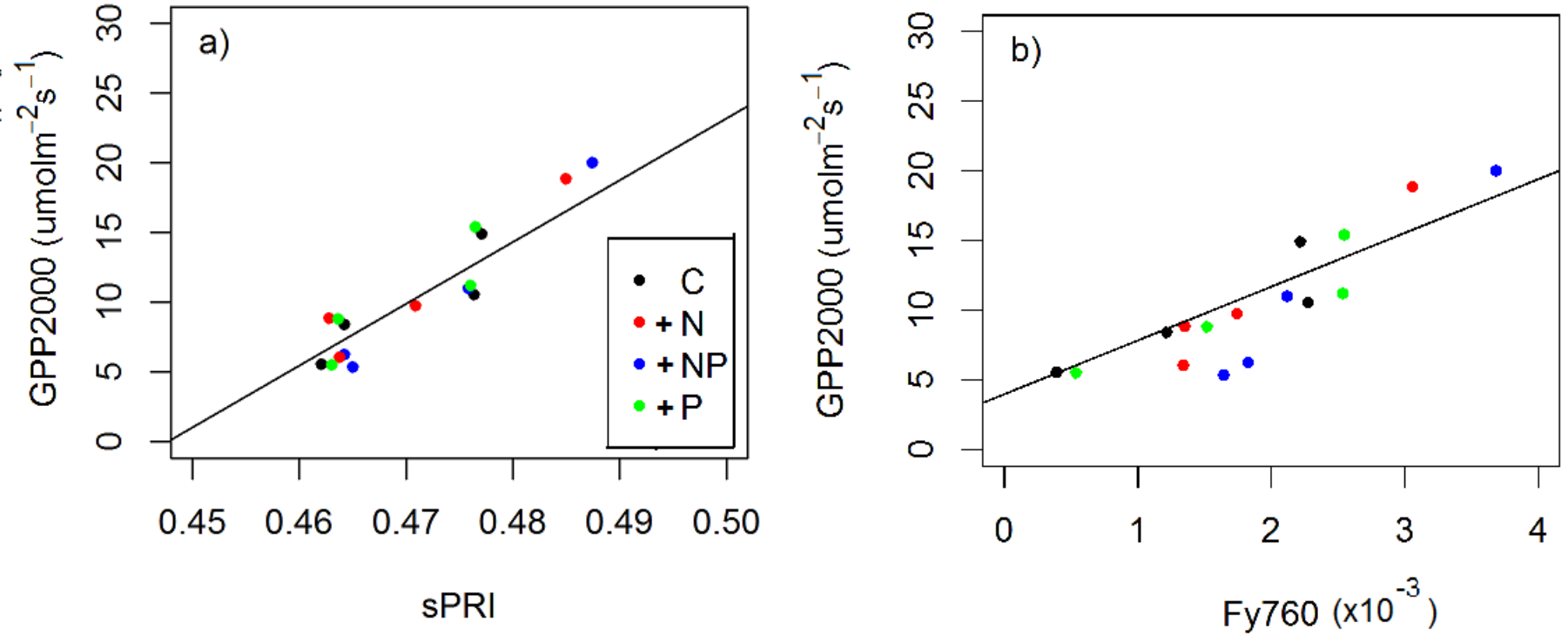
a)
GPP2000 (umolm^{-2}s^{-1})
0
5
10
15
20
25
30
0.45
0.46
0.47
0.48
0.49
0.50
sPRI
C
+ N
+ NP
+ P
b)
GPP2000 (umolm^{-2}s^{-1})
0
1
2
3
4
Fy760 (x10^{-3})

Fig. 5

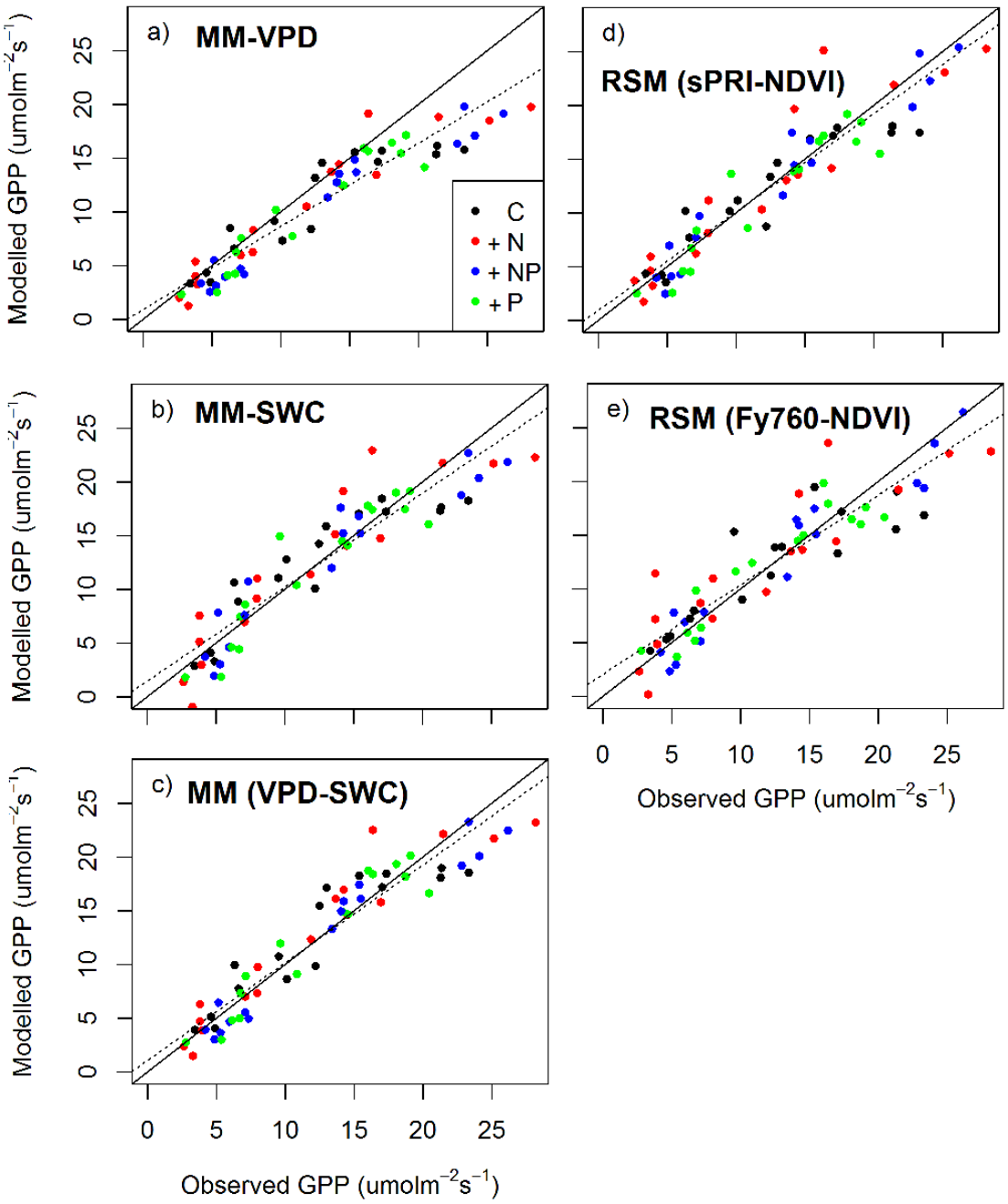
a) MM-VPD
b) MM-SWC
c) MM (VPD-SWC)
d) RSM (sPRI-NDVI)
e) RSM (Fy760-NDVI)
C
+ N
+ NP
+ P
Modelled GPP (umolm^{-2}s^{-1})
Observed GPP (umolm^{-2}s^{-1})
0
5
10
15
20
25

Fig. 6

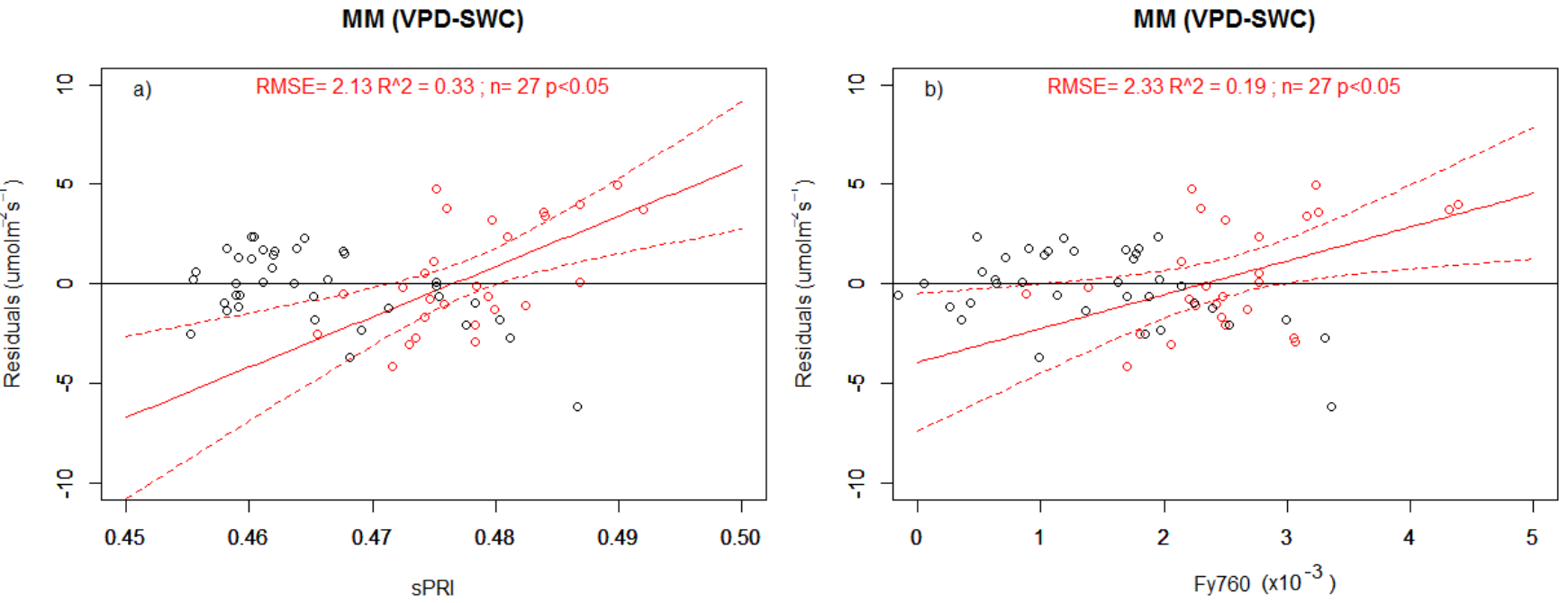
MM (VPD-SWC)
a)
RMSE= 2.13 R^2 = 0.33 ; n= 27 p<0.05
Residuals (umolm-2s-1)
10
5
0
-5
-10
0.45
0.46
0.47
0.48
0.49
0.50
sPRI
MM (VPD-SWC)
b)
RMSE= 2.33 R^2 = 0.19 ; n= 27 p<0.05
Residuals (umolm-2s-1)
0
1
2
3
4
5
Fy760 (x10-3)

Fig. 7

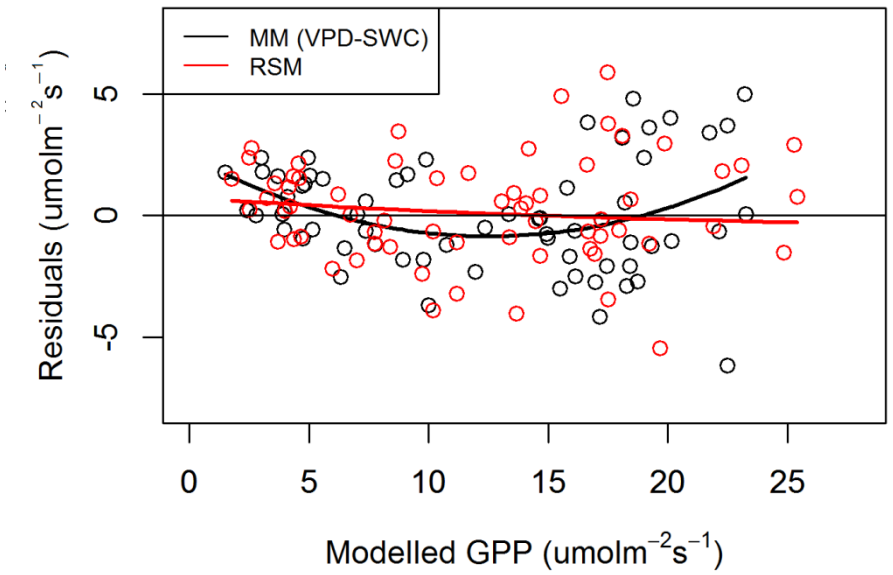
MM (VPD-SWC)
RSM
Residuals (umolm^{-2}s^{-1})
5
0
-5
0
5
10
15
20
25
Modelled GPP (umolm^{-2}s^{-1})

Fig. 8

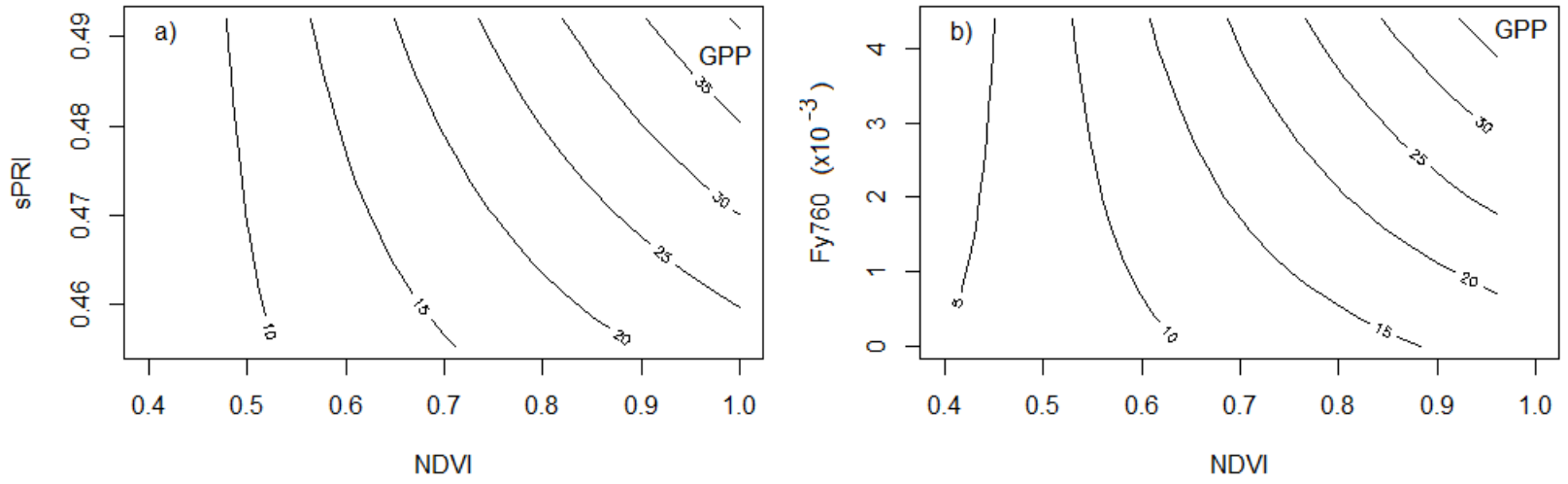
a)
GPP
sPRI
0.46
0.47
0.48
0.49
0.4
0.5
0.6
0.7
0.8
0.9
1.0
NDVI
10
15
20
25
30
35
b)
GPP
Fy760 (x10 -3)
0
1
2
3
4
NDVI
5
10
15
20
25
30

Fig. 9